THESIS FOR THE DEGREE OF DOCTOR OF PHILOSOPHY

Electrochromic Plasmonic Metasurfaces for Reflective Displays

Kunli Xiong

CHALMERS

Department of Chemistry and Chemical Engineering
CHALMERS UNIVERSITY OF TECHNOLOGY
Göteborg, Sweden 2017

Electrochromic Plasmonic Metasurfaces for Reflective Displays

Kunli Xiong

ISBN 978-91-7597-657-0

Doktorsavhandlingar vid Chalmers tekniska högskola

Ny serie nr 4338

ISSN 0346-718X

Department of Chemistry and Chemical Engineering

SE-412 96 Göteborg

Sweden

Telephone +46(0)72-9371508

Email xiongkunli1987@gmail.com

Cover:

Top left: Nanostructure for plasmonic color generation

Top right: Different colors made of plasmonic materials

Bottom: The image “The Weeping Woman” painted by Pablo Picasso made of plasmonic pixels.

Chalmers Bibliotek, Reproservice

Göteborg, Sweden 2017

Electrochromic Plasmonic Metasurfaces for Reflective Displays
Kunli Xiong
Department of Chemistry and Chemical Engineering
Chalmers University of Technology

Abstract

Plasmonic nanomaterials provide brilliant colors that arise from the ambient light coupling to the free electrons in metals. In the Roman empire, noble metal nanoparticles were used for staining glass in Church windows and tableware. Thanks to the extra-long lifetime of the plasmonic nanoparticles such glasswork still looks equally bright in color and can thus be used even after thousands of years. In comparison with organic dyes or paints, plasmonic nanomaterials provide strong stable colors even in ultrathin materials (hundreds of nanometers). If the colors can be electrically controlled this provides a novel technology for display devices.

In recent years, reflective (paper-like) displays become more and more interesting since they provide clear images in illuminated environments and are more friendly for human eyes compared to emissive display devices (LED, LCD). One of the most successful commercialized electronic papers is the E-ink technology (e.g. the popular KindleTM). However, one big problem of the E-ink technology on the market is that it only displays monochromatic text or pictures.

It has been known for some time that by implementing electrochemical control over the plasmonic nanostructures one can actively tune the optical response to some extent. Recently, it has also been shown that when combining conjugated polymers with the plasmonic nanomaterials the optical transmission can be modulated with high contrast and fast response speed.

In our work, a novel plasmonic nanomaterial combined with conjugated polymers works as an “electronic paper” in color with high contrast, fast response time (ms) and ultra-low power consumption ($0.5 mW/cm^2$). In particular, by using an ultrathin plasmonic nanostructure with a soft polymer layer the system is highly bendable with ultra-high optical reflection (>90 %), which opens up for a new technology for electronic paper applications.

Keywords: Colors; Electronic paper; Plasmons; Conductive polymers.

Publications

List of papers included in this thesis:

Paper 1: A thermal plasmonic sensor platform: Resistive heating of nanohole arrays.

K. Xiong & M. Virk, M. Svedendahl, M. Käll, A. B. Dahlin. **Nano Letters 2014**, 14 (6), 3544–3549.

I did the simulation of the temperature distribution and fabricated the plasmonic materials. I also finished the sensor related experiments.

Paper 2: Biosensing using plasmonic nanohole arrays with small, homogenous and tunable aperture diameters.

K. Xiong, G. Emilsson, A.B. Dahlin. **Analyst 2016**, 141 (12), 3803-3810.

I did the simulation and the experiment of measuring the plasmonic signals. Meanwhile, I fabricated the plasmonic materials.

Paper 3: Plasmonic metasurfaces with conjugated polymers for flexible electronic paper in color.

K. Xiong, G. Emilsson, A. Maziz, X. Yang, L. Shao, E.W.H. Jager, A.B. Dahlin.
Advanced Materials 2016, 28 (45), 9956-9960.

I proposed the idea and finished the simulation, fabrication, and experiments of this paper.

Paper 4: Switchable plasmonic metasurfaces with high chromaticity containing only abundant metals.

K. Xiong, D. Tordera, G. Emilsson, O. Olsson, U. Linderhed, M.P. Jonsson, A. B. Dahlin.
Nano Letters (accepted).

I proposed the idea and finished the simulations and experiments of this paper. I also fabricated the color generators in this paper.

List of papers not included in this thesis:

Fabrication and characterization of plasmonic nanopores with cavities in the solid support. K. Xiong & B. Malekian, G. Emilsson, J. Andersson, C. Fager, E.M. Larsson-Langhammer, A.B. Dahlin. Sensors 2017, 7 (6), 1444.

Plasmonic nanopores in metal-insulator-metal films. A. B. Dahlin, M. Mapar, K. Xiong, F. Mazzotta, F. Höök, T. Sannomiya. **Advanced Optical Materials 2014**, 2 (6), 556–564.

Plasmon enhanced internal photoemission in antenna-spacer-mirror based Au/TiO2 nanostructures. Y. Fang, Y. Jiao, K. Xiong, R. Ogier, Z.-J. Yang, S. Gao, A.B. Dahlin, M. Käll. **Nano Letters 2015**, 15 (6), 4059–4065.

Location-specific nanoplasmonic sensing of biomolecular binding to lipid membranes with negative curvature. J. Junesch, G. Emilsson & K. Xiong, S. Kumar, T. Sannomiya, H. Pace, J. Vörös, S.-H. Oh, M. Bally, A.B. Dahlin. **Nanoscale 2015**, 7 (37), 15080-15085.

Surface plasmon resonance methodology for monitoring polymerization kinetics and morphology changes of brushes - evaluated with poly(N-isopropylacrylamide). G. Emilsson, R.L. Schoch, P. Oertle, K. Xiong, R.Y.H. Lim, A.B. Dahlin. **Applied Surface Science 2017**, 396, 384-392.

Contents

Chapter 1 **Introduction to Displays**

In modern life, it is hard for people to live without displays! Television, smartphones and computers take up as much as 10 hours per day of our time and most likely even more in the future. A lot of people have to use displays for work and they are required for many types of entertainment. In recent years, it has become quite common that people stare at their cell phone screen on the bus, subway or even while driving because of the development of 3G/4G technology. The evolution of display technologies started from Monochrome Cathode Ray Tube (MCRT) displays in 1922 [1]. Images are first converted into an electrical signal by the iconoscope or camera tube. The cathode ray is deflected by a magnetic field based on the electrical signal and excites a fluorescent material for displaying the images on the screen. The Color Cathode Ray Tube (CCRT) was developed in the 1950s. It started to utilize red, green and blue (RGB) pixels to display images or videos in color. However, it is hard to make a portable CCRT screen because of the complicated mechanism and ultra high energy consumption (>250 mW/cm^2) [2].

The idea of using liquid crystals for display applications was conceived in 1963 [3]. In that period, the concept of "TV-on-a-wall" was still a dream for the Television pioneers. Unlike CRT technology, LCD screens do not use phosphor, which suffers image "burn-in" when a static image is displayed on a screen for a long time. Much lower electrical power consumption enables LCD to use batteries as the power source, which is one important requirement for making portable devices. LCD displays are mainly comprised of a backlight source, color filters, polarizers and liquid crystals. The backlight source emits white light that can transform into red, blue and green colors after passing through the color filters and the liquid crystals control the on/off states of each pixel together with the polarizers. Similarly to CRT technology, images are first transformed into electrical signals that control the on/off states of each pixel, thereby displaying an image on the screen. Because of the low power consumption and thinner device structure (compared to CRT), LCD realized the dream of commercializing portable displays.

One of the biggest disadvantages of LCD is that the viewing angle is limited. The contrast of the colors decreases with higher viewing angles. Light-emitting diode (LED) displays provide an efficient way to solve this problem. LEDs was developed in the 1960s as an outgrowth of semiconductor technology [4].

The devices emit light when a bias voltage is applied to a p-n junction in the group III-V compounds. By doping different kinds of III-V materials, it is possible to produce specific emission of red, green and blue light. In comparison to LCD, LED is also thinner and has a longer lifetime, which makes LED popular for cell phones, tablets or ultra-thin screens. In recent years, the organic light-emitting diode (OLED) is used in flexible electronic devices [5]. Different with traditional LED made by semiconductors, OLED is made of organic materials which are electrically conductive due to the delocalization of pi electrons caused by conjugation over all or parts of the molecules. In comparison to traditional LED, OLED is thinner and lighter. However, the lifetime is shorter and the maximum power of luminescence is lower.

CRT, LCD and LED are emissive display technologies, which have to emit light for showing pictures or movies. Emissive display technologies are friendly in a dark environment since the contrast between the screen and environment can be quite high. However, the contrast drops a lot if the emissive display is used in a bright environment. That is why people need to increase the brightness of the screen a lot for reading in sunshine. Another problem with emissive displays is that they need a large amount of energy to keep emitting photons. For a normal smartphone, the screen consumes more than 80% of the power (~20 mW/cm^2) of the battery and the power consumption becomes even higher in strong illumination conditions (i.e. daylight). The ratio between emitted and electric power has already been optimized to ~ 30% (LEDs). Even by obtaining 100% conversion efficiency, it would still correspond to too high energy consumption. Hence, reflective displays, which promote a big step towards saving energy for electronic displays, have been invented and become more and more popular in the modern life.

Reflective displays, also called “electronic paper”, reflect the light from the environment for displaying pictures or movies. They consume much less electricity compared with emissive display technologies since they do not emit any light at all. Only a little bit of energy is required to switch the state of each pixel and reflective displays can potentially display static images with essentially zero power consumption, although no display has reached this goal yet. Electrophoretic displays (EPD) is the most known reflective display technology, made by Eink, which is used in Kindle^{TM} electronic book reader

(Amazon). EPD utilizes control of the black (absorbing) or white (reflective) states of the dichromatic electronic inks to display texts or images. The texts or images of EPD will not disappear even without charging, which is different with other emissive displays. The most energy is consumed in switching and it needs a high voltage (~100V) to drive the switching fast enough for reading. Still, the greatest limitation of regular EPDs is the monochromatic display, which limits the applicability of the technology. The special colorful EPD has been made but no products can be purchased right now.

The only one commercialized colorful reflective display is Reflective Liquid Crystal Display (RLCD). Instead of using backlight, RLCD reflects the light from the environment as the EPD for display. RLCD is using red, green and blue (RGB) pixels triplets to generate colors and only a fraction of the area is typically active, i.e. maximum 33% for the respective color. Also, half of the light intensity is lost when the light needs to pass through a polarizer, which means only the reflected light from the environment is low. The low reflectivity will result in poor contrast in the pixels since the “on” state is not very bright to begin with. Another big problem of RLCD is the limitation of viewing angle due to the relatively thick (mm) liquid crystal layers, which also means RLCD can not be flexible.

This thesis describes a novel flexible electronic paper in color, which is made by plasmonic metasurfaces with conjugated polymers[6]. The principle of the colorful display is similar to RLCD and the RGB colors are generated by different nanostructures for different colors. Conjugated polymers are used to modulate the on/off states of the plasmonic metasurface. In comparison to electrochromic polymers alone, this overcomes the weak chromaticity of the polymers. In addition, the thickness of the polymers is ultrathin (hundreds of nanometers) which overcomes the disadvantage of LCD, so an ultra high-resolution display can be achieved in principle and it still take advantage of the fact that the polymer only needs very low power. The flexible plasmonic metasurface is even thinner than the polymer layer but it can create highly intense coloration (>90% resonant absorption or reflection). Overall, the new kind of plasmonic-polymer electronic papers can provide a high chromaticity display with high contrast, fast response time (ms) and ultra-low power consumption (0.5 mW/cm^2). Chapter 2 will introduce the physical theory of plasmons and describe plasmonic modes in different structures. In Chapter 3, a review of different plasmonic color generators is presented. Nanofabrication of plasmonic materials is introduced in

Chapter 4. A review of conjugated polymers as the reflection modulator and the electrochemical control is introduced in Chapter 5. Last, Summary and Future outlook are discussed in Chapter 6.

Chapter 2 **Maxwell’s Equations and electromagnetic wave functions**

This Chapter focuses on the introduction of physical theory about plasmons. It starts with analyzing Maxwell’s Equations and Electromagnetic wave functions, which are the basic theories for describing plasmonic modes in nanostructured metallic materials. Then, the formulas of Drude model and the dielectric function of metals are derived. They are used to describe the optical properties of metals and dielectrics. After the above basic theory description, more details about the plasmonic modes of nanoparticles and nanoholes structures are introduced. All these theories provide mathematic technologies to analyze, describe and improve the plasmonic metamaterials for color generators.

2.1 Maxwell’s Equations and electromagnetic wave functions

Maxwell’s Equations describe the electromagnetic response both of idealized and real metals over a wide frequency range and introduce the fundamental excitation of the conduction electron “sea” in bulk metals, so-called plasmons. In our case, they can be used for analyzing the optical properties of different nanostructures and metals. Based on Maxwell’s Equations, the transmission, reflection or scattering of the nanomaterials can be simulated to design the specified geometries of nanostructures to generate different colors. First, one can consider Maxwell’s Equations of macroscopic electromagnetism in the following form [7]:

$$\nabla \cdot \mathbf{D} = \rho_{ext} \tag{2.11a}$$

$$\nabla \cdot \mathbf{B} = 0 \tag{2.11b}$$

$$\nabla \times \mathbf{E} = -\frac{\partial \mathbf{B}}{\partial t} \tag{2.11c}$$

$$\nabla \times \mathbf{H} = \mathbf{J}_{ext} + \frac{\partial \mathbf{D}}{\partial t} \tag{2.11d}$$

In Equation 2.11a, **D** is the dielectric displacement, which can be derived from electrical field **E** in equition 2.12a. ρ_{ext} is the external charge. The equation means a motion along the electrical field will introduce the external charges in the material. In equation 2.11b, **B** is the magnetic field. The equation means that motion along the magnetic field will not introduce any charge. Equation 2.11c describes how a motion across the electrical field will introduce a change of magnetic field. In equation 2.11d, **H** is the magnetization field. Similarly, **H** is derived from magnetic field **B**. The equation describes how the motion across the magnetic field will introduce an electrical current and a variation in the electrical field.

The relations between **E**, **D** and **B**, **H** are presented by equations 2.12.

$$\mathbf{D} = \varepsilon_0 \mathbf{E} + \mathbf{P} \tag{2.12a}$$

$$\mathbf{H} = \frac{1}{\mu_0}\mathbf{B} - \mathbf{M} \tag{2.12b}$$

In the equations 2.12, ε_0 and μ_0 are the electric permittivity and magnetic permeability of vacuum, **P** and **M** are the polarization and magnetization, respectively. In this thesis, I focus on non-magnetic media (dielectric or metals such as Ag, Au), so can ignore the magnetic response represented by **M**. **P** describes the electric dipole moment inside the material, caused by the alignment of microscopic dipoles with the electric field. It can be used to present the internal charge density via $\nabla \cdot \mathbf{P} = -\rho_{int}$, so the internal charge and current densities are linked by

$$\mathbf{J}_{\text{int}} = \frac{\partial \mathbf{P}}{\partial t} \tag{2.13}$$

Inserting equation (2.13) into 2.12a gives:

$$\nabla \cdot \mathbf{E} = \frac{\rho_{\text{tot}}}{\varepsilon_0} \tag{2.14}$$

In this equation (2.14), $\rho_{tot} = \rho_{int} + \rho_{ext}$ and it can also be written like $\nabla \cdot \varepsilon_0 \mathbf{E} = -\nabla \cdot \mathbf{P} + \nabla \cdot \mathbf{D}$. The equation (2.14) describes how the motion along the electrical field will introduce charges. This theory is always used to calculate the electrical power or energy. Under ideal conditions, I assume the material is linear, isotropic and nonmagnetic. One can define the constitutive relations:

$$\mathbf{D} = \varepsilon_0 \varepsilon \mathbf{E} \tag{2.15a}$$

$$\mathbf{B} = \mu_0\mu\mathbf{H} \tag{2.15b}$$

ε is called the dielectric constant or relative permittivity and $\mu = 1$ the relative permeability of the nonmagnetic medium. In the equation 2.15a,

$$\varepsilon = 1 + \chi \tag{2.16a}$$

$$\mathbf{P} = \varepsilon_0\chi\mathbf{E} \tag{2.16b}$$

χ is the dielectric susceptibility, which is particularly used in quantum mechanics for analyzing the optical response. Last important relationship is that between internal current density **J** and the electric field **E**. They are linked by the conductivity σ:

$$\mathbf{J}_{\text{int}} = \sigma\mathbf{E} \tag{2.17}$$

It is obvious that there is a close relationship between ε and σ, which will be described here. In equation 2.13, $\partial/\partial t = -i\omega$ based on the Fourier domain. Normally, **E** can be described as $\mathbf{E} = Ae^{i(k\cdot\mathbf{r}-\omega t)}$ in traveling wave equation. A is the amplitude of the wave, k ($k = 2\pi/\lambda$, λ is the wavelength) is the spatial angular frequency (wavenumber) of the wave. ω ($\omega = 2\pi/T$, T is the period.) is the temporal angular frequency of the wave. **r** is the position. So equation 2.13 becomes:

$$\mathbf{J} = -i\omega\mathbf{P} \tag{2.18}$$

Inserting equation 2.18 into 2.17, I get:

$$\sigma\mathbf{E} = -i\omega\mathbf{P} \tag{2.19}$$

Inserting equation 2.19 into 2.16, I can get the fundamental relationship between the relative permittivity and the conductivity.

$$\varepsilon = 1 + \frac{i\sigma}{\varepsilon_0\omega} \tag{2.20}$$

Equation 2.20 is also called the dielectric function. Notably, especially for the interaction of light with metals, the response changes based on the spatial angular frequency of light, which is described by $\varepsilon(\omega)$. At low frequency, ε is usually used for describing the response of bound charges to a driving field, leading an electric polarization, while σ is the contribution of free charges to the current flow. In general, the dielectric function can be written as $\varepsilon(\omega) = \varepsilon_1(\omega) + i\varepsilon_2(\omega)$ and $\sigma(\omega) = \sigma_1(\omega)+i\sigma_2(\omega)$, which are complex valued functions of angular frequency ω. Then the complex refractive index becomes $n'(\omega) = n(\omega) + i\kappa(\omega)$, defined as $n'(\omega) = \sqrt{\varepsilon}$. Then, I can get

$$\varepsilon_1 = n^2 - \kappa^2 \tag{2.21a}$$

$$\varepsilon_2 = 2n\kappa \tag{2.21b}$$

$$n^2 = \frac{\varepsilon_1}{2} + \frac{1}{2}\sqrt{\varepsilon_1^2 + \varepsilon_2^2} \tag{2.21c}$$

$$\kappa = \frac{\varepsilon_2}{2n} \tag{2.21d}$$

κ is called the extinction coefficient, which represents the optical absorption of electromagnetic waves propagating through the medium. It is linked to the absorption coefficient α of Lambert-Beer's law by the relation

$$\alpha\,(\omega) = \frac{2\kappa(\omega)\omega}{c} \tag{2.22}$$

The exponential attenuation of the intensity of a beam propagating through the medium can be calculated by $I(x) = I_0 e^{-\alpha x}$. Based on equation 2.20, the absorption of the material is determined by the real part of σ, while the imaginary part contributes to the real part of the permittivity.

Now, I will introduce the wave equation. It is the traveling-wave solution of Maxwell's equations. Based on the equations 2.11c, 2.11d and 2.12b, it reads

$$\nabla \times \nabla \times \mathbf{E} = \nabla \times \left(-\frac{\partial \mathbf{B}}{\partial t}\right) = \nabla \times \left(-\mu_0 \frac{\partial \mathbf{H}}{\partial t}\right) = -\mu_0 \frac{\partial^2 \mathbf{D}}{\partial t^2} \tag{2.23}$$

Notice that in absence of external stimuli $\nabla \cdot \mathbf{D} = 0$. Still, if I assume the electrical field $\mathbf{E} = A\mathrm{e}^{\mathrm{i}\,(k\cdot\mathbf{r}-\omega t)}$, then

$$\nabla \times \nabla \times \mathbf{E} = -K^2\mathbf{E} + K(K \cdot \mathbf{E}) = -\mu_0\varepsilon_0\varepsilon\frac{\partial^2 \mathbf{E}}{\partial t^2} = -\varepsilon\frac{\omega^2}{c^2}\mathbf{E} \tag{2.24}$$

In equation 2.24, $c = \frac{1}{\sqrt{\mu_0\varepsilon_0}}$ is the speed of light in vacuum, K is propagation direction of the traveling-wave. For transverse waves, $K \cdot \mathbf{E} = 0$. Then the equation becomes

$$k^2 = \varepsilon \frac{\omega^2}{c^2} \tag{2.25}$$

However, for longitudinal waves, $\nabla \times \mathbf{E} = 0$. Based on equation 2.24, it leads to

$$\varepsilon(\omega) = 0 \tag{2.26}$$

2.2 Drude model and the dielectric function of metals

The Drude model explains the transport properties of electrons in materials [8]. It is mainly used to analyze the permittivity, conductivity and absorption coefficient of metals. This model assumes that the behavior of electrons in a solid is like a pinball machine, a lot of free electrons constantly hit the positive ions and bounce. The model is shown in figure 2.1.

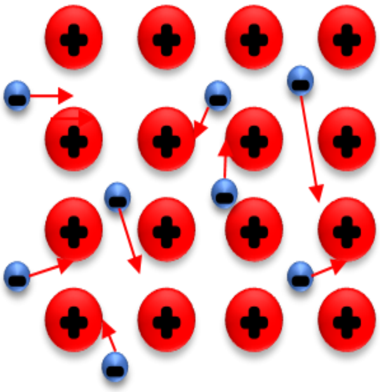

Figure 2.1. In Drude model, electrons constantly hit the positive ions (nucleus) and bounce. The blue particles are electrons and red particles are nuclei.

The basic Drude model is

$$m\ddot{\boldsymbol{x}} + m\gamma\dot{\boldsymbol{x}} = -e\mathbf{E} \tag{2.27}$$

This equation describes the motion of an electron of the plasma sea subjected to an external electric field $\mathbf{E}$. It can be assumed that the external electric field has a harmonic time dependence $\mathbf{E}(t) = \mathbf{E}_0 e^{-i\omega t}$. $\boldsymbol{x}$ is the oscillation of the electrons, m is the effective optical mass of each electron and γ is the collision frequency between nuclei and electrons, i.e. $\gamma = 1/\tau$ where τ is the relaxation time of the free electron gas. Normally, τ is on the order of 10^{-14} s at room temperature which corresponds to γ = 100 THz.

Equation 2.27 can be rewritten in another form

$$\frac{d\mathbf{P}(t)}{dt} = q\mathbf{E} - \frac{\mathbf{P}(\boldsymbol{t})}{\tau} \tag{2.28}$$

Since the $\boldsymbol{x}$ represents the oscillation of the electrons, $\dot{\boldsymbol{x}}$ is the velocity and $\ddot{\boldsymbol{x}}$ is the acceleration of the electrons. Based on the momentum equation $\mathbf{P} = mv = m\dot{\boldsymbol{x}} = \mathbf{F}t$, $\mathbf{F}$ is the applied force on the object, which in our case is the electron. v is the velocity of the electron. t is the time when the force is applied. In equation 2.27, $q\mathbf{E} = \mathbf{F}$. After one relaxation time, equation 2.27 transforms into

$$\tau \frac{d\mathbf{P}(t)}{dt} = \tau\,\mathbf{F} - \mathbf{P}(\boldsymbol{t}) \tag{2.29}$$

In equation 2.29, it is obvious that $\tau d\mathbf{P}(t)/dt = \tau m\ddot{\boldsymbol{x}} = m\Delta v = \Delta\mathbf{P}$, which is the momentum change of one electron, then equation 2.29 fulfils the momentum equation $\tau\,\mathbf{F} = \Delta\mathbf{P} + \mathbf{P}$. A particular solution of the equation 2.27 is $x(t) = x_0 e^{-i\omega t}$ since the oscillation of the electron follows the direction of the electrical force. After solving equation 2.27, this leads to

$$\boldsymbol{x}(t) = \frac{e}{m(\omega^2 + i\gamma\omega)}\mathbf{E}(t) \tag{2.30}$$

To solve equation 2.27, it can be assumed $\ddot{\boldsymbol{x}} = (-i\omega)^2\boldsymbol{x}$ and $\dot{\boldsymbol{x}} = (-i\omega)\boldsymbol{x}$, then $\boldsymbol{x}m(-\omega^2 - \gamma i\omega) = -e\mathbf{E}$. If the macroscopic polarization $\mathbf{P} = -ne\boldsymbol{x}$, where n is the amount of electrons, then

$$\mathbf{P} = -\frac{ne^2}{m(\omega^2 + i\gamma\omega)}\mathbf{E}(t) \tag{2.31}$$

Inserting the equation 2.31 into 2.12a yields

$$\mathbf{D} = \varepsilon_0\left(1 - \frac{\omega_p^2}{\omega^2 + i\gamma\omega}\right)\mathbf{E}(t) \tag{2.32}$$

where $\omega_p^2 = \frac{ne^2}{\varepsilon_0 m}$ is defined as the *plasma frequency* of the free electron gas. Therefore, it is obvious that the dielectric function becomes

$$\varepsilon = 1 - \frac{\omega_p^2}{\omega^2 + i\gamma\omega} \tag{2.33}$$

Since the complex dielectric function $\varepsilon(\omega) = \varepsilon_1(\omega) + i\varepsilon_2(\omega)$,

$$\varepsilon_1 = 1 - \frac{\omega_p^2\tau^2}{1 + \omega^2\tau^2} \tag{2.34a}$$

$$\varepsilon_2 = \frac{\omega_p^2\tau}{\omega(1 + \omega^2\tau^2)} \tag{2.34b}$$

Based on equation 2.33, $\varepsilon(\omega) = 1 - \frac{\omega_p^2 \cdot \omega^2}{\omega^4 + \gamma^2\omega^2} + \frac{i\gamma\omega\omega_p^2}{\omega^4 + \gamma^2\omega^2}$. After inserting $\gamma = \frac{1}{\tau}$, $\varepsilon(\omega) = 1 - \frac{\omega_p^2}{\omega^2\tau^2 + 1} + \frac{i\gamma\omega_p^2}{\omega(\omega^2\tau^2 + 1)}$. Normally the collision time is around 10^{-14}s and the plasma frequency is around 1000 THz (10^{15}). For $\omega\tau \gg 1$, the region of very high frequency, it leads to negligible damping.

$$\varepsilon_1(\omega) = 1 - \frac{\omega_p^2}{\omega^2} \tag{2.35a}$$

$$\varepsilon_2(\omega) = \frac{1}{\omega\tau} \approx 0 \tag{2.35b}$$

Then $$\varepsilon(\omega) = 1 - \frac{\omega_p^2}{\omega^2} \tag{2.35c}$$

Considering the regime of very low frequencies, where $\omega\tau \ll 1$. Then

$$\varepsilon_1(\omega) = 1 - \omega_p^2\tau^2 \tag{2.36a}$$

$$\varepsilon_2(\omega) = \frac{\omega_p^2\tau}{\omega} \tag{2.36b}$$

Notice that if $\frac{\omega_p}{\omega} \gg 1$, I assume that $\varepsilon_2 \gg \varepsilon_1$, and the real and the imaginary parts of the complex refractive index become

$$n = \sqrt{\frac{\varepsilon_2}{2}} = \sqrt{\frac{\omega_p^2\tau}{2\omega}} \tag{2.37a}$$

(2.37b)

$$\kappa = \frac{\varepsilon_2}{2n} = \sqrt{\frac{\varepsilon_2}{2}}$$

Inserting 2.37b into equation 2.22, the absorption coefficient α becomes

$$\alpha\,(\omega) = \frac{2\kappa(\omega)\omega}{c} = \sqrt{\frac{2\omega_p^2\tau\omega}{c^2}} \tag{2.38}$$

By introducing the expression of conductivity $\sigma_0 = \frac{ne^2\tau}{m} = \omega_p^2\tau\varepsilon_0$

$$\alpha = \sqrt{2\sigma_0\omega\mu_0}. \tag{2.39}$$

Where $c = \frac{1}{\sqrt{\varepsilon_0\mu_0}}$. Now, I introduce a new concept: Skin depth. When the electrical field is applied, the electron motions are largest near the surface of the conductor and decrease with the depth into the conductor. The skin depth means the distance between the surface and a level inside where the free electrons cease moving. In our case, the electrical fields fall off inside the metal as $\mathbf{E} = \mathbf{E}_0 e^{-z/\delta}$. Skin depth δ is defined as the depth below the surface of the conductor at which the electrical field falls to $1/e$ (about 0.37) of $\mathbf{E}_0$. The formula of the skin depth is:

$$\delta = \frac{2}{\alpha} = \frac{c}{\kappa\omega} = \sqrt{\frac{2}{\sigma_0\omega\mu_0}} \tag{2.40}$$

The formula is valid as long as the mean free path of the electrons $l = v_F\tau \ll \delta$, where v_F is the Fermi velocity (the highest speed of electrons). Normally, for typical metals $l \approx 10\ nm$ and $\delta \approx 100\ nm$.

Last, I will consider our specific materials, the metals (e.g. Au, Ag, Cu, Al). Equations 2.34 describe the free-electron model and $\varepsilon \to 1$ at $\omega \gg \omega_\mathrm{p}$. For the noble metals, it has a highly polarized environment. By adding the term $\mathbf{P}_\infty = \varepsilon_0(\varepsilon_\infty - 1)\mathbf{E}$ to equation 2.12a, it reads

$$\mathbf{D} = \varepsilon_0\mathbf{E} - \frac{ne^2}{m(\omega^2 + i\gamma\omega)}\mathbf{E} + \varepsilon_0(\varepsilon_\infty - 1)\mathbf{E} \tag{2.41a}$$

Then

$$\varepsilon = \varepsilon_0\varepsilon_\infty - \frac{ne^2}{m(\omega^2 + i\gamma\omega)} = \varepsilon_\infty - \frac{\omega_p^2}{\omega^2 + i\gamma\omega} \tag{2.41b}$$

In equation 2.41, ε_∞ is a dielectric constant that describes the polarized environment in metals. Specially, for the colorful metals (Au, Cu, Al etc), the interband transitions occur in a part of the visible light, leading to increase κ (high absorption). That is why gold has yellow color and copper has red color. Last but not the least, the expression for the AC conductivity $\sigma = \frac{ne\mathbf{p}}{m}$, $\mathbf{P} = m\dot{\boldsymbol{x}}$ and $\sigma_0 = \frac{ne^2\tau}{m}$

$$\sigma = ne\dot{\boldsymbol{x}} = \frac{-i\omega\tau ne^2}{m(\omega^2\tau + i\omega)} = \frac{\sigma_0}{1 - i\omega\tau} \tag{2.42}$$

Inserting equation 2.42 into the permittivity expression 2.33 gives

$$\varepsilon = 1 + \frac{i\sigma}{\varepsilon_0\omega} \tag{2.43}$$

2.3 Nanoparticle plasmons

Nanoparticles can naturally scatter an oscillating electromagnetic field and the incident electromagnetic field can drive the electrons of the nanoparticles to generate a restoring electrical force. The oscillations lead to a resonance between the electrons and incident field, which amplify the electrical field both inside and in the near-field zone outside the particle, especially for certain frequencies. The resonance is called the *localized surface plasmon resonance* (LSPR). For the metallic nanoparticles (gold, silver, etc), the resonance falls into the visible region of the electromagnetic spectrum. The nanoparticles can scatter and absorb specific wavelengths of light, which makes nanoparticles exhibit bright colors both in transmitted and reflected light.

I start with a simple model: a nanosphere with d as the diameter illuminated by a light beam with angular frequency ω. The particle size is much smaller than wavelength ($d < \lambda$) and the dielectric constant of the surrounding medium is ε_m. The permittivity of the metallic sphere is described by the dielectric function $\varepsilon(\omega)$. In a static field, the gradient of the field is zero $\nabla\mathbf{E} = 0$, then $\nabla^2\phi = 0$, where ϕ is the potential since $\nabla\phi = \mathbf{E}$.

To solve this model, Maxwell's equations reduce to Laplace's equation in spherical symmetry. The solution is the form [7].

$$\phi(r,\theta) = \sum_{l=0}^{\infty}\left[A_l r^l + B_l r^{-[l+1]}\right]P_l(cos\theta) \tag{2.44}$$

where $P_l(cos\theta)$ are the legendre polynomials of order l. θ is the angle between the position vector r at point P and the axis of the external field. Based on Figure 2.3, the potentials $\boldsymbol{\phi}_{\text{in}}$ inside and $\boldsymbol{\phi}_{\text{out}}$ outside the sphere can be written as:

$$\boldsymbol{\phi}_{\text{in}}(r,\theta) = \sum_{l=0}^{\infty} A_l r^l P_l(cos\theta) \tag{2.45}$$

$$\boldsymbol{\phi}_{\text{out}}(r,\theta) = \sum_{l=0}^{\infty}\left[B_l r^l + C_l r^{-(l+1)}\right]P_l(cos\theta) \tag{2.46}$$

It should be noticed that $\boldsymbol{\phi}_{\text{in}} = 0$ based on Faraday's law of induction when $r < 0$, so $A_l = 0$. However, A_l can be defined at the sphere surface $r = a$. Because the electric field is continous at the boundary, the tangential and normal components of the electric field demand that

$$\frac{1}{a}\frac{\partial\boldsymbol{\phi}_{\text{in}}}{\partial\theta} = \frac{1}{a}\frac{\partial\boldsymbol{\phi}_{\text{out}}}{\partial\theta} \tag{2.47a}$$

$$-\varepsilon_0\varepsilon_m\frac{\partial\boldsymbol{\phi}_{\text{in}}}{\partial r} = -\varepsilon_0\varepsilon_m\frac{\partial\boldsymbol{\phi}_{\text{in}}}{\partial r} \tag{2.47b}$$

where ε_m is the permittivity of the environment. Before I get the expression of the potentials, I should notice that $\boldsymbol{\phi}_{\text{out}}(r,\theta) = B_l r P_l(cos\theta) = -E_0 r cos\theta$ as $r \to \infty$ since $C_l r^{-(l+1)} \to 0$. The expression becomes [7]:

$$\boldsymbol{\phi}_{\text{in}} = -\frac{3\varepsilon_0}{\varepsilon + 2\varepsilon_m}E_0 r\cos\theta \tag{2.48a}$$

$$\boldsymbol{\phi}_{\text{out}} = -E_0 r\cos\theta + \frac{\mathbf{P}\cdot\mathbf{r}}{4\pi\varepsilon_0\varepsilon_m r^3} \tag{2.48b}$$

In equations 2.48, $\mathbf{P}$ is the dipole moment of the applied field and the particle center. $\mathbf{P} = 4\pi\varepsilon_0\varepsilon a^3 \frac{\varepsilon-\varepsilon_0}{\varepsilon+2\varepsilon_m}\mathbf{E}_0$. Similar to equation 2.16b, I can introduce the polarizability α to describe the dipole moment $\mathbf{P} = \varepsilon_0\varepsilon_m\alpha\mathbf{E}_0$, then

$$\alpha = 4\pi a^3 \frac{\varepsilon - \varepsilon_m}{\varepsilon + 2\varepsilon_m} = V\frac{\varepsilon - \varepsilon_m}{\varepsilon + 2\varepsilon_m} \tag{2.49}$$

where V is the volume of the sphere. The polarizability implies a resonant enhancement of both the internal and dipolar field and the radiation of the dipole leads to scattering of a plane wave by the sphere. In fact, the resonantly enhanced polarization α is an enhancement both in scattering and absorbing light. The cross section for the scattering and absorption can be described by [9]

$$C_{sca} = \frac{k^4}{6\pi}[\alpha]^2 = \frac{8\pi}{3}k^4a^6\left[\frac{\varepsilon - \varepsilon_m}{\varepsilon + 2\varepsilon_m}\right]^2 \tag{2.50a}$$

$$C_{abs} = \frac{k^4}{6\pi}[\alpha]^2 = \frac{8\pi}{3}k^4a^6\left[\frac{\varepsilon - \varepsilon_m}{\varepsilon + 2\varepsilon_m}\right]. \tag{2.50b}$$

It is obvious that the efficiency of absorption is much higher than the scattering efficiency for small particles ($a \ll \lambda$) and the polarizability has a resonant enhancement under the condition that $|\varepsilon + 2\varepsilon_m|$ is at a minimun. The resonance then simplifies to $Re[\varepsilon(\omega)] = -2\varepsilon_m$.

Finally, the extinction cross section is defined as $C_{ext} = C_{sca} + C_{abs}$, it reads:

$$C_{ext} = 9\frac{\omega}{c}\varepsilon_m^{3/2}V\frac{\varepsilon_2}{[\varepsilon_1 + 2\varepsilon_m]^2 + \varepsilon_2^2} \tag{2.51}$$

The extinction cross section is the effective area of the shadow of the particle when illuminated by light. The extinction reaches a maximum when the polarizability has a resonant enhancement.

2.4 Surface Plasmonic Polaritons at Metal-Insulator Interfaces

In this section, I focus on describing the plasmonic modes at metal-insulator interfaces, which is the basic theory to analyze the nanoholes structures used in this work. Generally, I can design different geometries of nanohole structures (diameter, periodicity, thickness, etc.) to reflect different colors. The plasmonic wave propagation at the interface between a dielectric and a conductor is called Surface Plasmon Polaritons (SPP). When the incident light couples to the conductor's electron plasma, the SPP wave is excited and the electron plasma oscillates in the direction perpendicular to the interface.

In section 2.11, I described Maxwell's Equations and wave functions. In order to investigate the physical properties of SPP, I apply the wave equation to the flat interface between a conductor and a dielectric. From equation 2.23, I know that

$$\nabla \times \nabla \times \mathbf{E} = -\mu_0 \frac{\partial^2 \mathbf{D}}{\partial t^2} \tag{2.52}$$

Using the identities $\nabla \times \nabla \times \mathbf{E} = \nabla(\nabla \cdot \mathbf{E}) - \nabla^2 \mathbf{E}$ and I assume the SPP propagates perpendicular to the direction of the electrical field (electron oscillation). Then $\nabla \cdot \mathbf{E} = \mathbf{0}$ and I get:

$$\nabla^2 \mathbf{E} - \frac{\boldsymbol{\varepsilon}}{\boldsymbol{c}^2} \frac{\partial^2 \mathbf{E}}{\partial t^2} = 0 \tag{2.53}$$

To solve the equation, I still assume the $\mathbf{E}(t) = \mathbf{E}_0 e^{-i\omega t}$, then it reads:

$$\nabla^2 \mathbf{E} + k_{\mathbf{0}}^{\mathbf{2}} \boldsymbol{\varepsilon} \mathbf{E} = 0 \tag{2.54}$$

In the equation 2.54, $k_0 = \frac{\omega}{c}$, it is the wave vector of the propagating wave in vacuum. Equation 2.54 is called *Helmholtz equation* [10].

A single interface between a metal and a dielectric layer is the simplest geometry to sustain SPPs. The model is shown in Figure 2.2. The top half part ($\mathrm{z} > 0$) is a metal layer described by a dielectric function $\varepsilon_1(\omega)$ which is described by equation 2.33. The bottom layer ($\mathrm{z} < 0$) is a dielectric with positive real dielectric constant ε_2. I describe the SPP wave function based on Maxwell equations, the SPP is confined to the interface and the propagation direction is X and electron oscillations are in the Y direction.

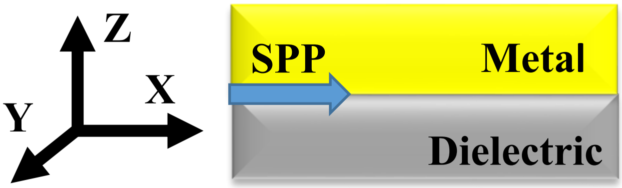

Figure 2.2. SPP propagation at a single interface between a dielectric and a metal. The oscillation direction is Z and the propagation direction is X.

First, I start with a TM wave. For the TM wave, there is no magnetic field in the wave propagation direction. In our case, the propagation is in X direction so the system can be seen as only having $\mathbf{H}_y$, $\mathbf{E}_x$ and $\mathbf{E}_z$. Based on equation 2.11d, I can conclude that the relationship between the electrical field and the magnetic field is

$$\nabla \times \mathbf{H} = \frac{\partial \mathbf{D}}{\partial t} = \varepsilon\varepsilon_0 \frac{\partial \mathbf{E}}{\partial t} = -i\omega\varepsilon\varepsilon_0 \mathbf{E} \tag{2.55}$$

Based on the right-hand rule, it leads to

$$-\frac{\partial \mathbf{H_y}}{\partial z} + \frac{\partial \mathbf{H_z}}{\partial y} = -i\omega\varepsilon\varepsilon_0 \mathbf{E_x} \tag{2.56a}$$

$$\frac{\partial \mathbf{H_y}}{\partial x} - \frac{\partial \mathbf{H_x}}{\partial y} = -i\omega\varepsilon\varepsilon_0 \mathbf{E_z} \tag{2.56b}$$

Since $\mathbf{H}_x = 0$ and $\mathbf{H}_z = 0$

$$-\frac{\partial \mathbf{H_y}}{\partial z} = -i\omega\varepsilon\varepsilon_0 \mathbf{E_x} \tag{2.57a}$$

$$\frac{\partial \mathbf{H_y}}{\partial x} = -i\omega\varepsilon\varepsilon_0 \mathbf{E_z} \tag{2.57b}$$

Returning to the model again, since the wave propagates along X direction and oscillates along the Z direction, for the region $z > 0$, it can be derived that

$$\mathbf{H}_y(z) = A_m e^{i\beta x} e^{-k_m z} \tag{2.58a}$$

$$\mathbf{E}_x(z) = iA_m \frac{1}{\omega\varepsilon_m\varepsilon_0} k_m e^{i\beta x} e^{-k_m z} \tag{2.58b}$$

$$\mathbf{E}_z(z) = -A_m \frac{\beta}{\omega\varepsilon_m\varepsilon_0} e^{i\beta x} e^{-k_m z} \tag{2.58c}$$

Then, for the region $z < 0$, it can be derived that

$$\mathbf{H}_y(z) = A_d e^{i\beta x} e^{k_d z} \tag{2.59a}$$

$$\mathbf{E}_x(z) = -iA_d \frac{1}{\omega\varepsilon_d\varepsilon_0} k_d e^{i\beta x} e^{k_d z} \tag{2.59b}$$

$$\mathbf{E}_z(z) = -A_d \frac{\beta}{\omega\varepsilon_d\varepsilon_0} e^{i\beta x} e^{k_d z} \tag{2.59c}$$

Where β is the propagation constant, A_m is the amplitude of oscillation in the metal, A_d is the amplitude of oscillation in the dielectric, k_m is the wavevector in the metal and k_d the wavevector in the dielectric.

Since SPP is continuous, $\mathbf{H}_y$ is the same for the equations in both regions when $z = 0$. Then I can conclude that

$$A_d e^{i\beta x} = A_m e^{i\beta x} \tag{2.60a}$$

$$A_d = A_m \tag{2.60b}$$

For the same reason, when $z = 0$, $\mathbf{E}_x$ is the same, so

$$-\frac{k_d}{\varepsilon_d} = \frac{k_m}{\varepsilon_m} \tag{2.61a}$$

$$-\frac{k_d}{k_m} = \frac{\varepsilon_d}{\varepsilon_m} \tag{2.61b}$$

Returning to the wave function, equation 2.54 is derived from TE mode. Similarly, it is clear that for TM mode, the wave function becomes

$$\nabla^2\mathbf{H} + k_{\mathbf{0}}^{\mathbf{2}}\varepsilon\mathbf{H} = 0 \tag{2.62}$$

For the TM wave, $\nabla^2\mathbf{H} = \frac{\partial^2\mathbf{H}_y}{\partial x^2} + \frac{\partial^2\mathbf{H}_y}{\partial z^2} = (i\beta)^2\mathbf{H}_y + \frac{\partial^2\mathbf{H}_y}{\partial z^2}$ since the magnetic field only has $\mathbf{H}_y$ and $\frac{\partial\mathbf{H}_y}{\partial y} = 0$, inserting it into 2.62 gives

$$(i\beta)^2\mathbf{H}_y + \frac{\partial^2\mathbf{H}_y}{\partial z^2} + k_{\mathbf{0}}^{\mathbf{2}}\varepsilon\mathbf{H}_y = 0 \tag{2.63a}$$

$$\frac{\partial^2\mathbf{H}_y}{\partial z^2} + (k_{\mathbf{0}}^{\mathbf{2}}\varepsilon - \beta^2)\mathbf{H}_y = 0 \tag{2.63b}$$

Based on equation 2.63b, for $z > 0$, $\frac{\partial^2\mathbf{H}_y}{\partial z^2} = k_m^2\mathbf{H}_y$ and for $z < 0$, $\frac{\partial^2\mathbf{H}_y}{\partial z^2} = k_d^2\mathbf{H}_y$, yielding

$$k_m^2 = \beta^2 - k_{\mathbf{0}}^{\mathbf{2}}\varepsilon_m \tag{2.64c}$$

$$k_d^2 = \beta^2 - k_{\mathbf{0}}^{\mathbf{2}}\varepsilon_d \tag{2.64c}$$

After solving this equation, I can get the wavevector of SPP, notice that $-\frac{k_d}{k_m} = \frac{\varepsilon_d}{\varepsilon_m}$.

$$\beta = k_0\sqrt{\frac{\varepsilon_d\varepsilon_m}{\varepsilon_d + \varepsilon_m}} \tag{2.65}$$

I can use a similar way to analyze the TE mode. Based on Maxwell's equations, $\nabla \times \mathbf{E} = i\omega\mu_0\mathbf{H}$ and only $\mathbf{E}_y$, $\mathbf{H}_x$ and $\mathbf{H}_z$ are nonzero.

For the region $z > 0$, it can be derived that

$$\mathbf{E}_y(z) = A_m \mathrm{e}^{i\beta x}\mathrm{e}^{-k_m z} \tag{2.66a}$$

$$\mathbf{H}_x(z) = -iA_m\frac{1}{\omega\mu_0}k_m\mathrm{e}^{i\beta x}\mathrm{e}^{-k_m z} \tag{2.66b}$$

$$\mathbf{H}_z(z) = A_m\frac{\beta}{\omega\mu_0}\mathrm{e}^{i\beta x}\mathrm{e}^{-k_m z} \tag{2.66c}$$

and for the region $z < 0$

$$\mathbf{E}_y(z) \ = \ A_d \mathrm{e}^{i\beta x} \mathrm{e}^{k_d z} \tag{2.67c}$$

$$\mathbf{H}_x(z) = iA_d \frac{1}{\omega\mu_0} k_d \mathrm{e}^{i\beta x} \mathrm{e}^{-k_d z} \tag{2.67b}$$

$$\mathbf{H}_z(z) = A_d \frac{\beta}{\omega\mu_0} \mathrm{e}^{i\beta x} \mathrm{e}^{-k_d z} \tag{2.67c}$$

Still, at the interface $z = 0$, $\mathbf{E}_y$ and $\mathbf{H}_z$ are continuous, which leads to

$$A_m \mathrm{e}^{i\beta x} = A_d \mathrm{e}^{i\beta x} \tag{2.68a}$$

$$A_m = A_d \tag{2.68b}$$

$$-iA_m \frac{1}{\omega\mu_0} k_m = iA_d \frac{1}{\omega\mu_0} k_d \tag{2.68c}$$

$$A_d k_d + A_m k_m = 0 \tag{2.68d}$$

It is obvious that this condition is only fulfilled if $A_d = A_m = 0$ since $k_d > 1$ and $k_m > 1$. Thus, no surface modes exist for TE polarization. ***Surface plasmon polaritons only exist for TM polarization***.

Last, I will show how to derive the ***surface plasmon frequency***. In equation 2.65, when the propagation speed of the surface plasmon approaches infinity ($\beta \sim \infty$), $-\varepsilon_d = \varepsilon_m$. In the limit of negligible damping of the conduction electron oscillation ($\omega\tau \gg 1$), based on equation 2.35a, I get

$$\omega_{sp} = \frac{\omega_p}{\sqrt{1 - \varepsilon_m}} = \frac{\omega_p}{\sqrt{1 + \varepsilon_d}} \tag{2.69}$$

This mode is known as the ***surface plasmon***. It should be noticed that $\sqrt{\frac{\varepsilon_d \varepsilon_m}{\varepsilon_d + \varepsilon_m}} \gg 1$ since $\varepsilon_d + \varepsilon_m \approx 0$ and it means that $\beta > k_0$. The momentum of the incident light is $\frac{hk_0}{2\pi}$ (h is the Planck constant), which is smaller than the momentum of excited surface plasmon $\frac{h\beta}{2\pi}$, so the system does not fulfill the conservation of momentum and the surface plasmon cannot be excited. In next section, I will present one technology which overcomes the momentum problem to excite surface plasmon.

2.5 Plasmonic signal of short-range ordered nanoholes

In the last section, we have discussed the surface plasmon mode at the interface between a dielectric and a conductor. After a series of derivations, the propagation function of SPP in TM mode β and the angular frequency of the surface plasmon ω_{sp} are calculated. However, at the end of section 2.4, we mentioned that the system doesn't fulfill the conservation of momentum. This section presents how to utilize nanoholes in the metal layer to excite the surface plasmons.

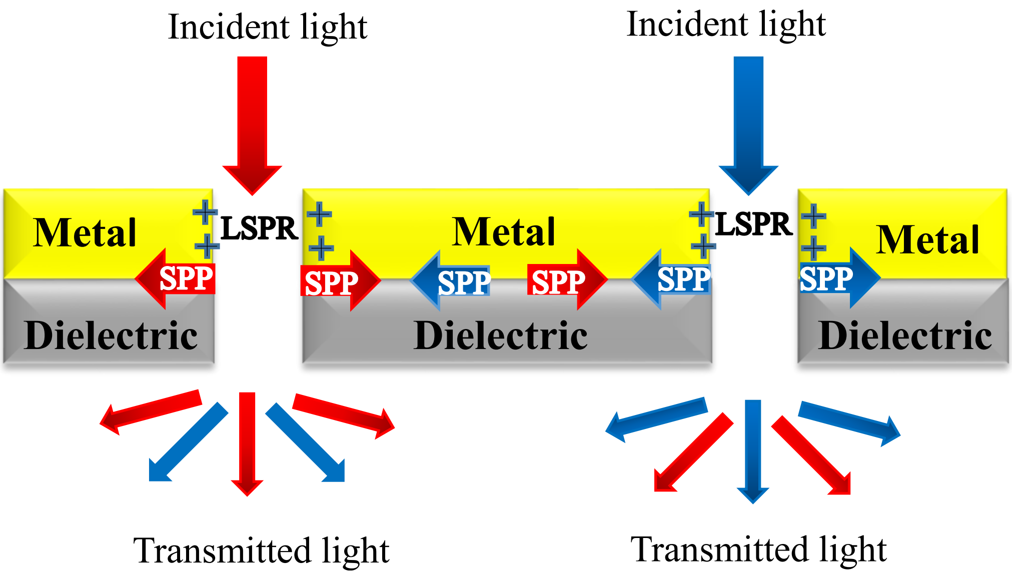

Figure 2.3. SPPs are excited when the incident light passes through the nanoholes. They can propagate along the interface between the metal layer and the dielectric layer. After reaching to the neighboring holes, SPPs can interfere with the incident light on the neighboring holes.

Fig. 2.3 shows how the plasmons are excited in the nanoholes structure by incident photons. When the photons reach the nanoholes surface, they can transform their momentum and energy into the electron oscillations of the metal. Some energy will be absorbed inside of the metal because of the collisions of the electrons inside. The other energy and momentum can be transported along the interface of the metal and dielectric, which would form the surface plasmonic polaritons (SPP) [11]. For the nanoholes structure, the SPP can travel from one hole to the neighboring hole along the interface, then the SPP can interfere with the incident light on the neighboring holes and change the intensity of the transmitted light.

We have discussed that the plasmons cannot be excited on a metal surface without a nanostructure because the momentum of incident photons is smaller than for the plasmons [12]. In equation 2.56, the wave vector, k_{spp}, of the SPPs with a wavelength λ depends on the dielectric function of the metal ε_m. The refractive index of the dielectric at that wavelength is n_d, according to the dispersion relation:

$$k_{spp} = \frac{2\pi}{\lambda}\sqrt{\frac{\varepsilon_m n_d^2}{\varepsilon_m + n_d^2}} \tag{2.61}$$

where $\frac{2\pi}{\lambda} = k_0$ is the wave vector in a vacuum. The incident photon travels in the air with the refractive index n_0 ($n_0 \approx 1$). The component of the wave vector which is parallel to the planar metal/dielectric interface is:

$$k_{photon} = \frac{2\pi}{\lambda} n_0 sin(\theta) \tag{2.62}$$

where θ is the angle of incidence. If the photon has normal incidence, k_{photon} would be 0. Even if the incidence angle is 90 degrees, so that k_{photon} will be $\frac{2\pi}{\lambda} n_0 < \frac{2\pi}{\lambda} n$, k_{spp} is still lager than k_{photon} since $\sqrt{\frac{\varepsilon_m n_d^2}{\varepsilon_m + n_d^2}} > n_0$ ($\varepsilon_m n_d^2 < \varepsilon_m + n_d^2 < 0$).

One of the most common ways to excite plasmons by normal incidence light is to fabricate periodic nanostructures which are smaller than the incident wavelength on the metal surface. The nanostructure can lead to scattering of the incident light, which can increase the component parallel to the metal surface of the photon momentum to excite the plasmons. For the nanoholes structure, the plasmons are excited at the nanoholes and form SPPs, which spread along the metal/dielectric interface. The new wave vector at normal incidence would then be:

$$k_{photon} = \frac{2i\pi}{\Lambda}$$

(2.63)

where Λ is the lattice constant and i is a nonzero integer number representing the scattering orders from the grating-like structure. Since the grating increases the momentum ($\Lambda \leq \lambda$) of the photons, the SPPs can be excited by an array of nanoholes. The SPPs can influence the extinction spectrum (transmitted light) of the nanoholes structures. Since SPPs can travel along the metal/dielectric interface and reach to the neighboring holes, there is interference with the incident photons on the neighboring nanoholes, which changes the extinction spectrum. Because of the half wave loss, if the phase of the SPPs is then equal to $2\pi i$ (i is integer number) of the incident photons phase, the transmitted light would be weakest, which is the peak position of the extinction spectrum. Thus, the wavelength of the peak position can be estimated by the function.

$$\Lambda = \frac{2\pi i}{\mathrm{Re}(k_{spp})} \tag{2.64}$$

where Λ is the average distance to the neighbor holes (periodicity). If only considering the condition i=1, then equation (2.64) would be $\Lambda = \lambda_{spp}$.

Fig. 2.4 shows the relationship between the λ_{SPP} and λ_{photon}, which is calculated based on the structure of a 30 nm gold film on a glass substrate. It should be noticed that this mode is not the same as only a

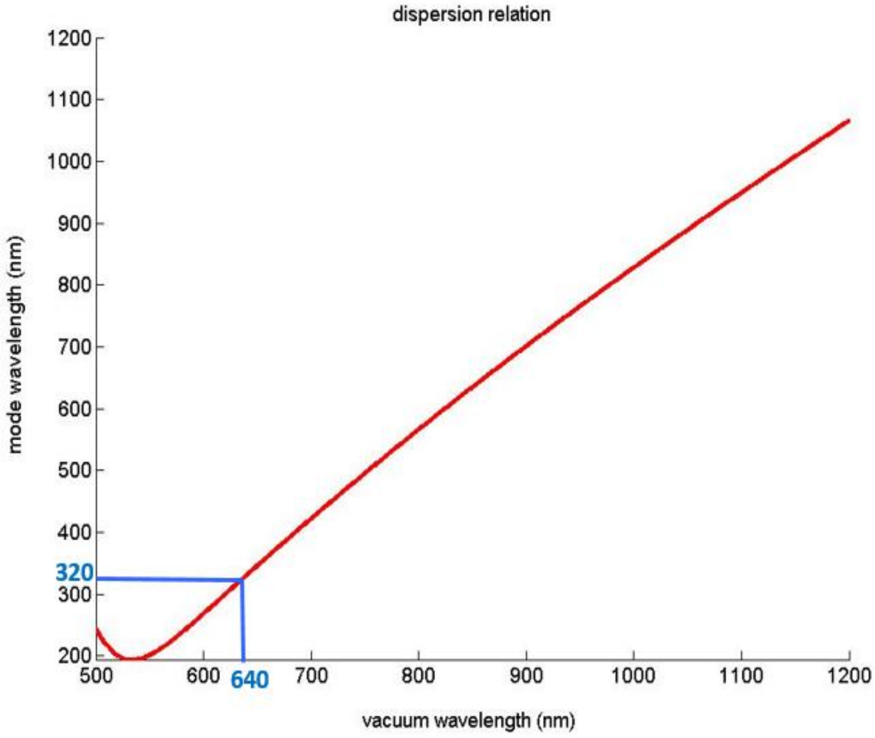

Figure 2.4. The relationship between the mode wavelenghth (λ_{spp}) and vaccum wavelength. (λ_{photon}).

single interface since the thickness of the gold film is finite. This mode considers both the thickness of gold layer and the interfaces of gold-air and gold-substrate. Since the permittivity of gold is not constant, the relationship is also not linear. In general, nanoholes with 158 nm diameter and 320 nm periodicity are used as the plasmonic sensor in this work. Base on the dispersion relation, when $\Lambda = 320$ nm, the peak position should be around 640 nm. Fig. 2.5 shows the extinction spectrum of the nanoholes sample.

In Fig. 2.5, it is quite clear that the peak position is around 650 nm, which is a little red shifted compared with the expected value. The error comes from the holes which change the permittivity of the metal [13]. It is quite clear in this view that the peak position of the extinction spectrum is mainly related with the periodicity of nanoholes. However, the dip position is mainly influenced by the diameter of nanoholes.

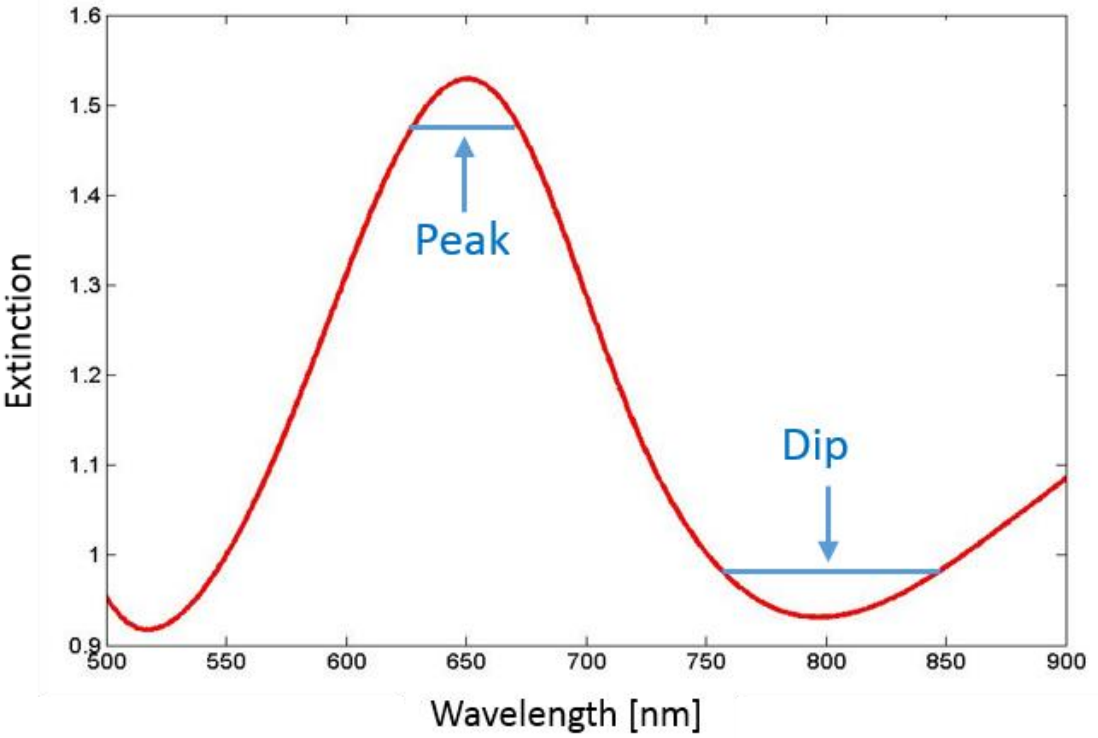

Figure 2.5. Plasmonic signal of nanoholes with 150 nm diameter, 320 nm periodicity and 30 nm thickness.

The Fig. 2.6 shows the extinction spectrum of different nanoholes samples. It is quite clear that the peak positions of different diameters nanoholes are almost the same, which are around 650 nm [14]. However, the dip positions have obvious blue shifts with decreasing diameters. In fact, the dip position is more related with the localized surface plasmon resonance (LSPR) [15], which can mainly decide the transmission of the incident light. Since LSPR is mainly decided by the hole sizes, the dip position varies with the diameters of the holes.

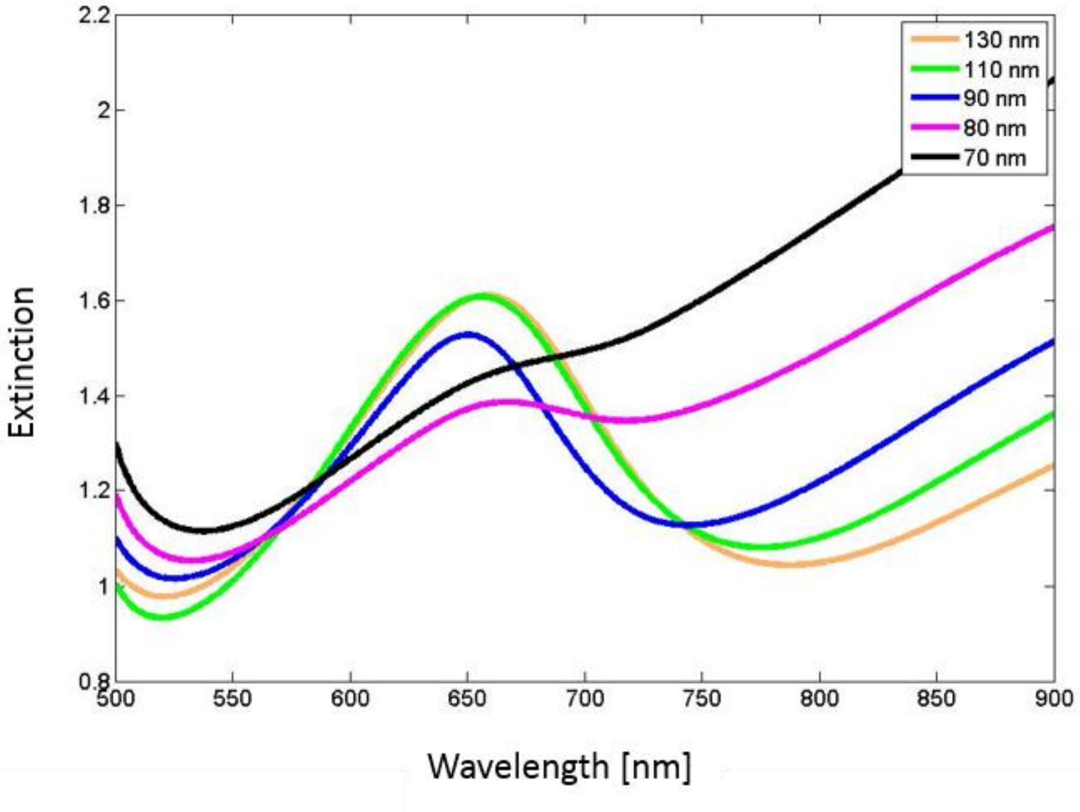

Figure 2.6. The spectrum of different nanoholes samples. The diameter changes from 130 nm to 70 nm. The periodicity is constant 320 nm and the gold thickness is 30 nm.

The wavelength of a photon with strongest LSPR could be calculated by the function

$$\mathrm{Re}\{\varepsilon_d + \mathrm{L}[\varepsilon(\lambda_{LSPR}) - \varepsilon_d]\} = 0 \tag{2.65}$$

where ε_d is the refractive index of the environment and L is a geometrical constant. Equation 2.65 is used to caculate the LSPR mode of nanodisks, $\mathrm{L} \propto h/D$, D is the diameter of the nanodisks, h is the thickness. Then, $\varepsilon\,(\lambda_{LSPR}) \propto h/D$ since $\varepsilon\,(\lambda_{LSPR}) < 0$ and $\lambda_{LSPR} \propto D/h$ since $\varepsilon(\lambda) = 1 - \frac{\omega_p^2}{2\pi}\frac{\lambda}{c} < 0$ for visible light. So the dip position should have a redshift with increased diameter of the nanodisks.

Nanohole structure have similar properties as the nanodisk, however, it is also influenced by the periodicity. I emphasize that a full understanding of the optical properties remains challenging and one should not interpret the peak and dip as two independent spectral features. Based on my study and these paper results [16] [17] [18], the dip position behaves like a localized resonance.

Besides the influence of the geometrical structure on the peak and the dip positions of the spectrum, the refractive index of the environment can also affect them. For an environment with higher refractive index, both the peak and the dip will red shift. Fig. 2.7 shows the relationship between the shifts and the refractive index of the environment. Nanohole samples with two different diameters, 60 nm and 160 nm are used. In this experiment, different water solutions with an increasing amount of glycerol (5, 10, 15, 20, 25, 30 and 35 percent by weight) are used to change the refractive index of the environment. With higher concentration, the refractive index will increase and cause linear red shifts on the peak and the dip positions. In Fig. 2.7B, it is quite clear that the amount of shifting for the peak and the dip is not very related with the diameter of the nanoholes.

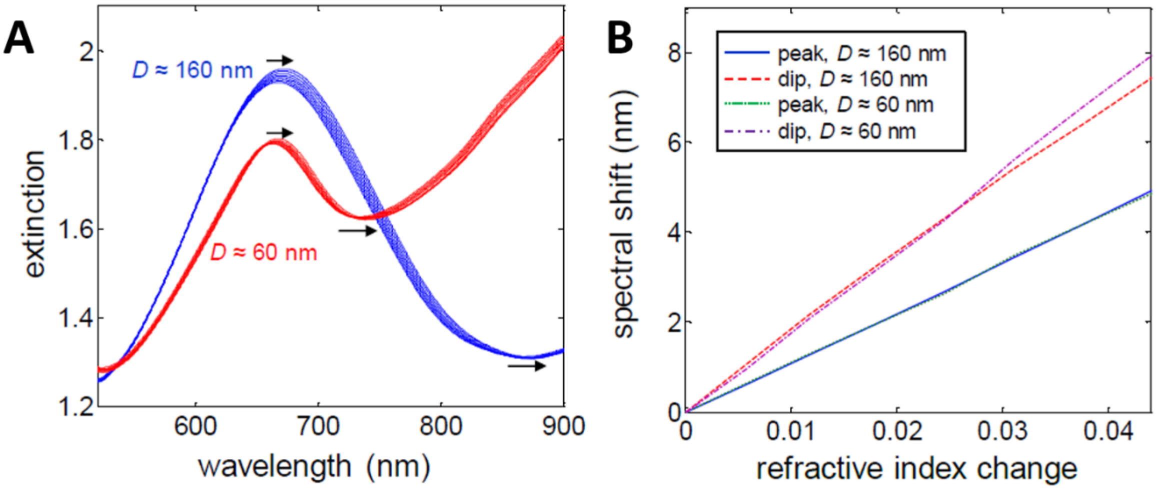

Figure 2.7. The relationship between the shifts and the refractive index of the environment.

Chapter 3 **Plasmonic color generation**

Stained glass had been used several thousand years ago for creating bright and permanent colors by utilizing plasmons [19]. Chromatic glass contains tiny proportions of nanoparticles of metals or metallic derivates scattering or absorbing visible light. One of the earliest and most known examples is the so called Lycurgus cup (Figure 3.1a) which is a Roman glass cup made in the 4th century. One interesting physical phenomenon is that the color of the cup changes from red to green depending on the direction of the light source luminance. It shows red color when lit from behind and green when lit from in front. This is because the stained glass of the Lycurgus cup has dichroic properties due to the surface plasmon resonances of the metallic nanoparticles in the glass. The nanoparticles can absorb the blue light, scatter the green light and transmit the red light.

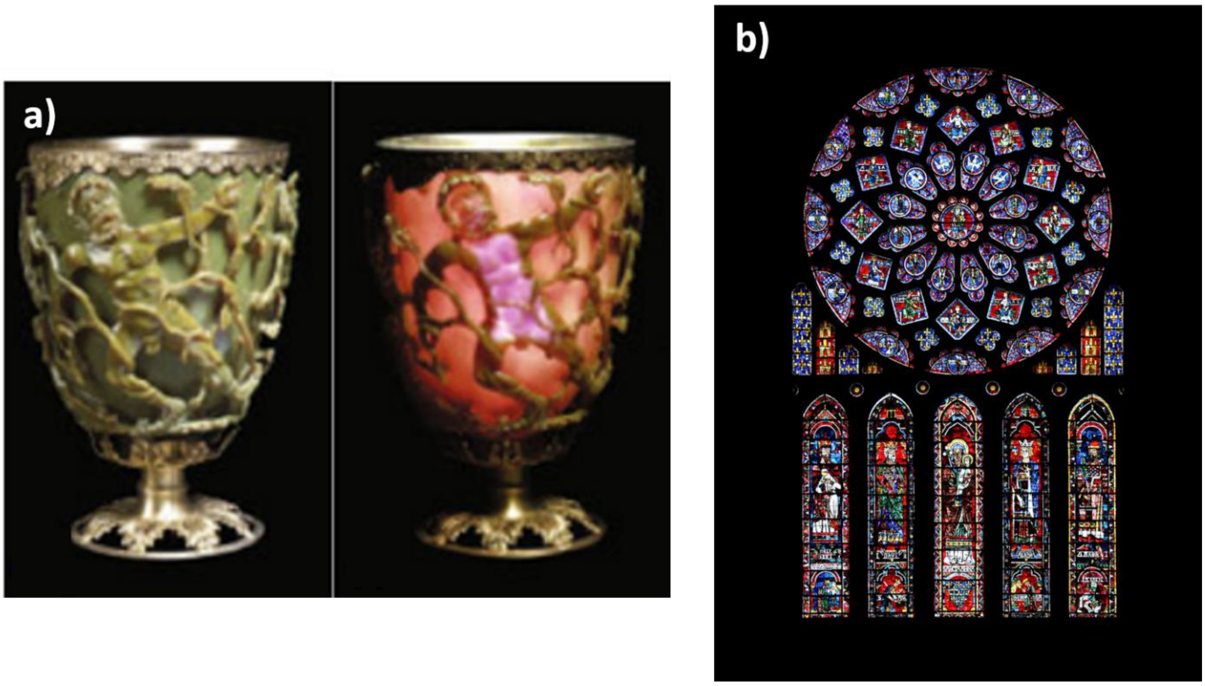

Figure 3.1. (a) The cup in reflected (left) and transmitted light (right) (b) The north transept rose of Chartres Cathedral is comprised by stained glass. The image is from reference [19].

Another widely used application for stained glasses is colored patterning the windows of churches (Figure 3.1b) [20], mosques and other significant buildings. In medieval Europe, the patterned windows made by stained glasses instead of painting pictures directly on the windows due to the lifetime of the colors of the stain glasses, which last as long as the glass itself. For getting strong colors different kinds of materials and sizes of the nanoparticles are used in the glass. The whiteness can also be adjusted by the concentration of the colloidal particles. Not only the metallic particles but also metallic derivates are used for creating colors. For instance, Iron (II) oxide can be used for green color and copper oxide produces turquoise color. The church windows are patterned by assembling lots of small pieces of chromatic stained glass on a rigid frame. By using this technology, the pictures made of stain glasses keep the brilliant colors even until now.

In the next sections, we will introduce different color generation technologies by using “modern plasmonic”. With the development of nanotechnology, different metallic nanostructures can be accurately fabricated and the scattering, reflection and transmission of the nanostructures can thereby be tuned in the visible light range [21]. In section 3.1 and 3.2, the basic theories and models are discussed and several representative structures are presented and analyzed.

3.1 Structural color from plasmonic nanodisk and metallic grating

As a 2D (one metallic layer) plasmonic material, nanodisks can be accurately fabricated by electron-beam lithography (EBL), focused ion beam (FIB) [22] and Hole-Mask colloidal lithography (HCL) [23]. The precise size-controlled plasmonic nanodisk can be used to scatter a specific visible wavelength just like a color filter [24]. By changing the geometry and size of the nanodisk, the scattered wavelength can be adjusted since it changes the dipole moment and localized surface plasmon resonances (LSPR) of the nanodisk [25]. With the geometry adjustment, the optical spectrum of the plasmonic nanodisk is different in different metals. Silver and aluminum are normally used for display purposes since their interband transitions are mainly in the UV region [26] [27]. The scattering spectra of aluminum nanodisks fabricated on UV-grade fused silica substrates is shown in Fig. 3.2, which is published by N.J. Halas group in reference [28]. As the diameter of the nanodisks increases (Fig. 3.2b), phase delay across the nanodisk causes a redshift of the plasmon resonance (Fig. 3.2a). The scattering spectra of the Al nanodisks is also calculated by the finite difference time domain (FDTD) method (Fig. 3.2c). Even though the nanodisks have some small geometrical defects, the experimental results do not have significant deviations from the simulation. To achieve the full visible colors scattering, the diameter of the Al nanodisk need to be accurately adjusted from 90 nm (purple) to 180 nm (red) with constant thickness ~ 35 nm. Comparing with conventional chemical pigments, the plasmonic Al nanodisks have much stronger interaction with light, which provide a novel display technology with ultra-high resolutions and an ultra-thin system.

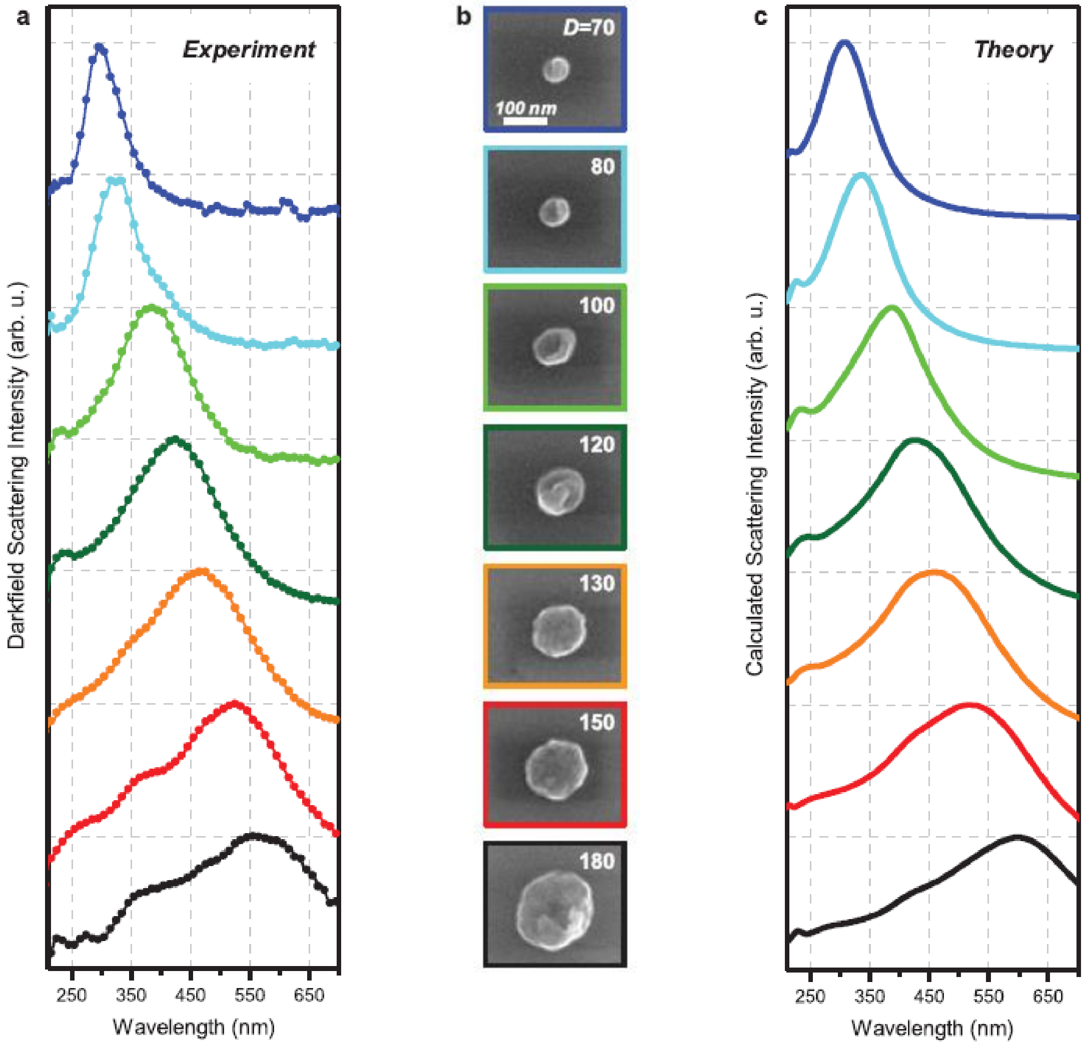

Figure 3.2. (a) Experimental dark-field spectra of individual nanodisks with D = 70, 80, 100, 120, 130, 150, 180 nm. (b) SEM micrographs of the corresponding nanodisk structures. Scale bar is 100 nm. (c) FDTD simulations of the nanodisk spectra, assuming a 3 nm surface oxide and a SiO2 substrate. The image is from reference [28].

Another 2D plasmonic nanostructure is grating-based nanorod array [29], which utilizes the diffraction phenomena to choose specific wavelengths of light to be transmitted or reflected from the material. Figure 3.3 shows how the plasmonic grating works. The incident light scatters from the periodic structure and excites LSPR modes on the silver nanowires. LSPR modes lead a phase delay which can interfere with the incident light thus influence the reflection and transmission. Since the optical signal is very sensitive to the periodicities of the grids, the grating structure is normally fabricated by EBL for its high accuracy [30].

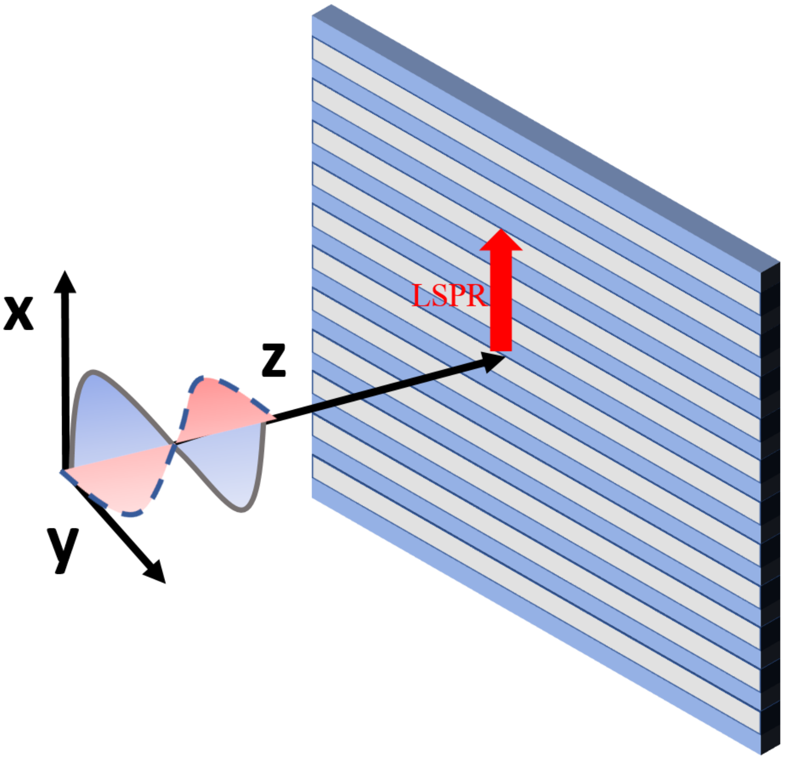

Figure 3.3. normal incident light containing TE and TM modes passes through the silver grid nanostructure, only TM mode can excite LSPR and lead to a phase delay.

Comparing with the nanodisk-based structure, one big difference is that the reflection and transmission of the grating-based displays is polarization dependent. LSPR can only be excited by the polarized light oscillating perpendicular to the grid direction, which means it can only work for 50% of the natural light since it contains both S (perpendicular) and P (parallel) polarizations.

Normally, grating-based nanostructure needs to work with polarizers for displays since the polarizer can filter out the incident light with the correct polarization. One of the most used materials is liquid crystals which are birefringent and can be modulated by applying voltages. Figure 3.4 shows how the transmitted colors change with different polarization of incident light, the image is published by L. Novotny group in reference [31]. In Figure 3.4, the transmission image is from grating-based silver grids with seven different thicknesses printed in different regions. The dimensions of the grids decide the LSPR mode which shows a strong resonance at a specific wavelength. Meanwhile, the colors can also be modulated by changing the polarization angle.

Figure 3.4. The image consists of silver grids with different thickness which generate different colors in different regions. The image is from reference [31].

3.2 Color generation from multilayer nanostructures

Comparing with a single layer plasmonic color generator, multilayer plasmonic nanostructures provides better quality colors and are normally used for reflection or scattering. Plasmonic nanodisks can be combined with a back-reflector to enhance the reflected color since this reflects the forward scattered light (Figure 3.5). Based on the multilayer nanodisk structure, color images can be printed with an extra high resolution which is ~100000 dots per inch [32]. The resolution of the traditional color printing based on ink deposition is limited by the size of each ink spot. Normally, the ink-spot sizes are around 25 μm which means the resolution is lower than 1000 DPI and it is already achieved in commercial laser printers. In figure 3.5, the diameter of the nanodisk is only around 100 nm which is the limit of the minimum size of the plasmonic pixels, thus the plasmonic images can reach an ultra high-resolution. To fabricate the multilayer plasmonic images, EBL which provides accurate size control is normally used since the colors of this structure are very sensitive to the diameter of the nanodisks.

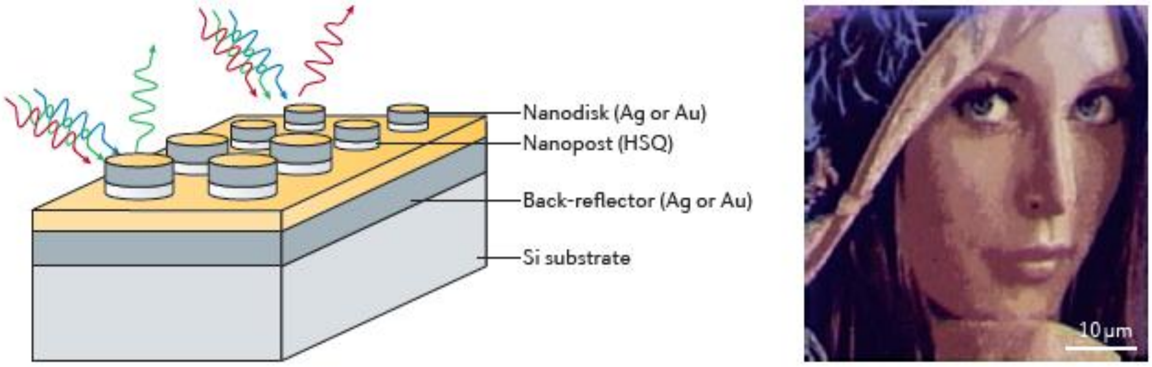

Figure 3.5. Multilayer plasmonic nanostructure is comprised by a back-reflector, HSQ (dielectric) and nanodisks. By changing the size of the nanodisks, different colors can be reflected back. The image is formed by printing different sizes of nanodisks in different regions. The image is from reference [32].

Recently, Anders Kristensen group tried to use a single-pulse laser to reshape the nanodisks to tailor the colors [33]. First, they printed multilayer nanodisks with the same size on a substrate, then a laser pulse of nanosecond duration is used to melt the nanodisks. Since the melting changes the morphology of the nanodisks, which shifts the resonant frequency of the LSPR, different colors can be generated. By controlling the parameters (power, spot size, etc) and the position of the laser pulse, different sizes of nanodisks can be patterned in different regions of the metasurface. Figure 3.6 shows how the system works and the image made by this technology.

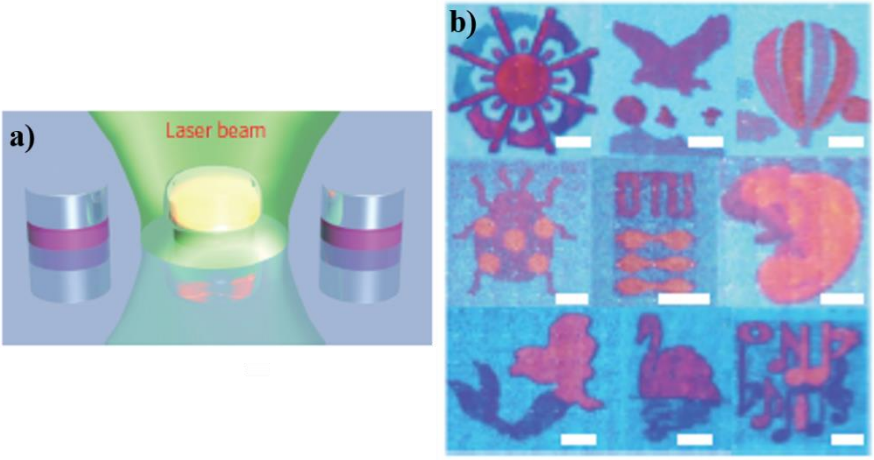

Figure 3.6. a) A schematic illustration of laser printing. b) Printed images in different color schemes. Scale bars: 5µm. The image is from reference [33]

Normally, the multilayer nanodisk structure needs a highly accurate fabrication technology since the colors are very sensitive to the geometry of the nanodisk. Thus, it is a big challenge to pattern these structures over a large area (like centimeter level). In this work we propose a novel multilayer nanohole structure to generate colors, which can be efficiently fabricated over tens of centimeters. The structure is shown in Figure 3.7.

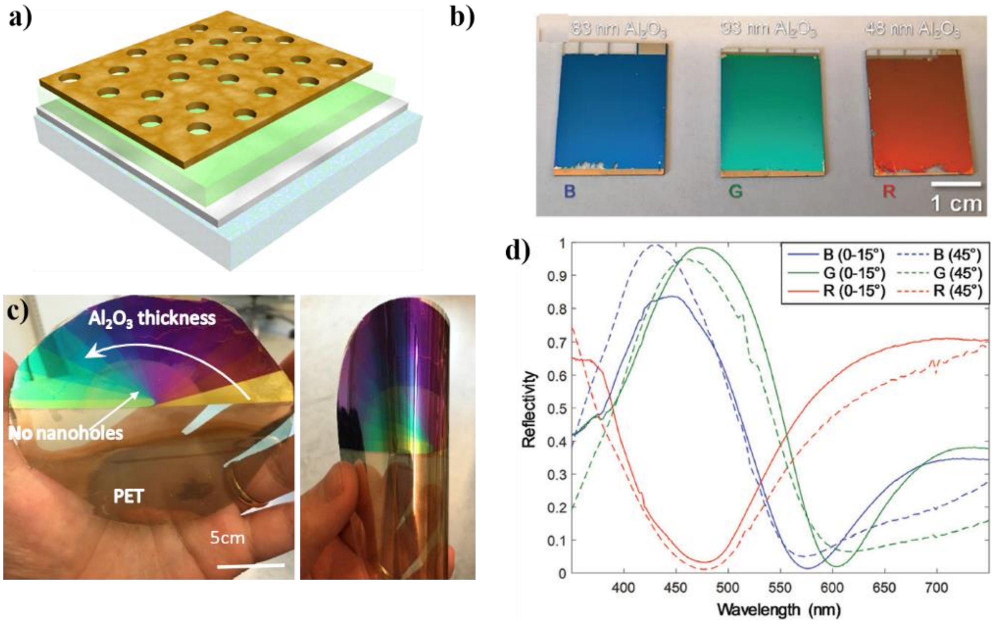

Figure 3.7. a) A schematic of the metasurface. b) A photo of samples with the primary colors under ambient light. c) A photo of a sample on polyethylene terephthalate (PET) support with a color palette generated by a gradient in alumina thickness. The middle region has no nanoholes in the gold film. d) Reflection spectra in air of the red, green, and blue samples for different angles.

Our metasurface also consists of three layers (Figure 3.7a). First, a silver reflector was deposited on the substrate and the subsequent alumina spacer layer is designed to tune the reflective color by Fabry-Pérot interference. Next, short-range ordered nanoholes in a gold film were prepared on alumina by colloidal lithography and tape stripping. Comparing with EBL or FBI, colloidal lithography consists of parallel processing steps compatible with large areas and plastic supports, which made the material flexible (Fig. 3.7c). More details about the colloidal lithography will be discussed in following sections. A color palette is fabricated by varying the alumina thickness and the high resonant reflectivity (~90%) (Fig. 3.7d) confirmed the clear colors of the nanomaterial (Fig. 3.7b).

Since the nanohole array structure can be fabricated over a large area and has a very high reflectivity, it can directly use the traditional RGB pixel triplets to generates chromatic images. RGB pixel triplets have been mentioned in the introduction part as the most common technology for all the commercialized displays. They can provide the largest color gamut by tuning the intensity of each pixel. For generating RGB colors, only utilizing the Fabry-Pérot interference between the top and bottom metallic layers is not enough. We need to fabricate the short-range ordered nanoholes to scatter away the redundant visible light. Figure 3.8 shows both the bright and dark fields of these RGB pixel triplets. By dark-filed illumination, we verified that the three RGB structures with nanoholes scattered their complementary colors at high angles. In order to show that the RGB pixel triplets can generate secondary colors, we produced microscale pixels of red, green and blue and patterned them in different regions.

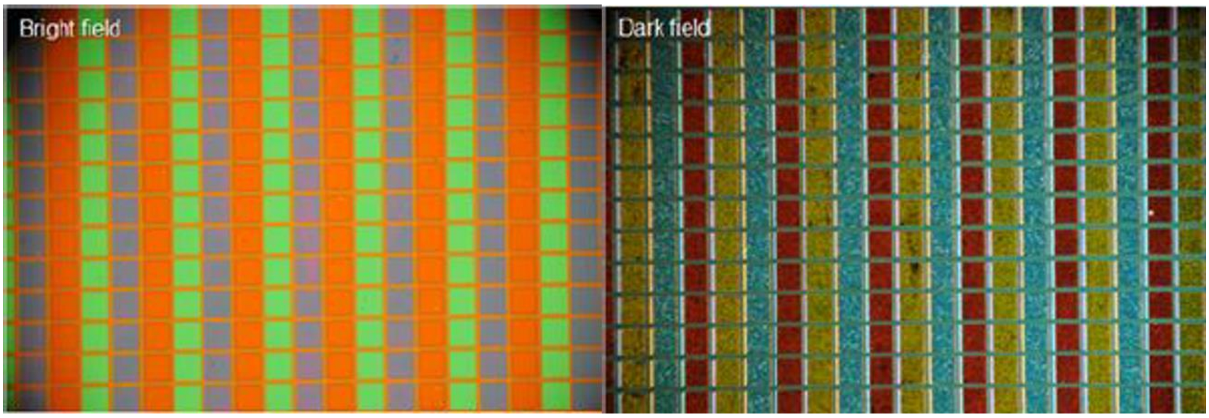

Figure 3.8. *The bright field and dark field of the RGB pixel triplets.*

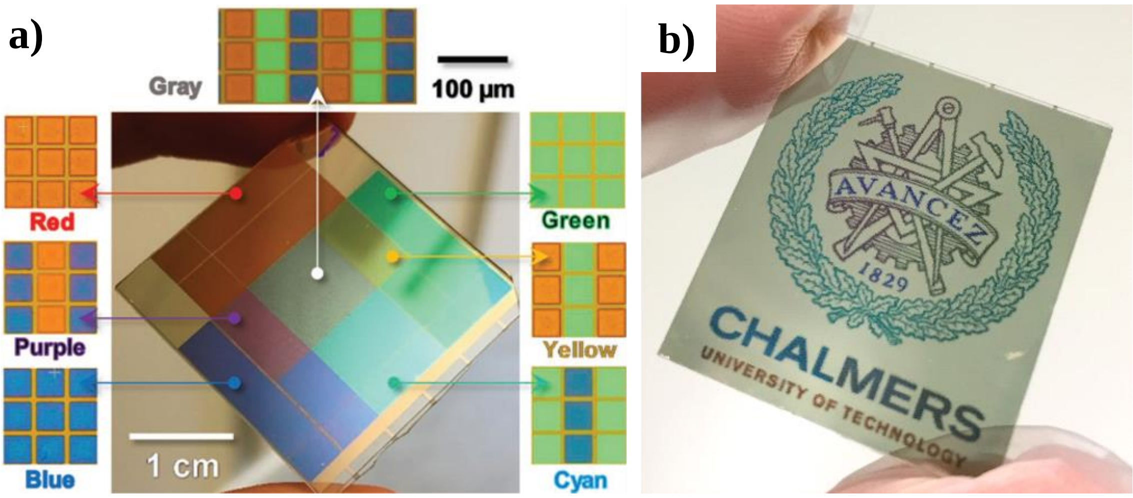

Figure 3.9. a) The secondary colors are generated. b) A sample with RGB pixels patterned to display the university logo in different colors.

Figure 3.9 shows how the secondary colors yellow, purple and cyan can be produced by their RGB combinations and a sample with RGB pixels patterned to display the University logo in different colors. For the above figures 3.7 to 3.9, the short-range ordered nanoholes are fabricated on the gold surface. In fact, the gold layer can be replaced by a copper layer. The price of copper is several thousand times lower than gold and the red color from the copper multilayer nanohole structure is better than the gold. Figure 3.10 shows the image of Lena formed by the copper based plasmonic pixels. The pixel size of each primary color is around

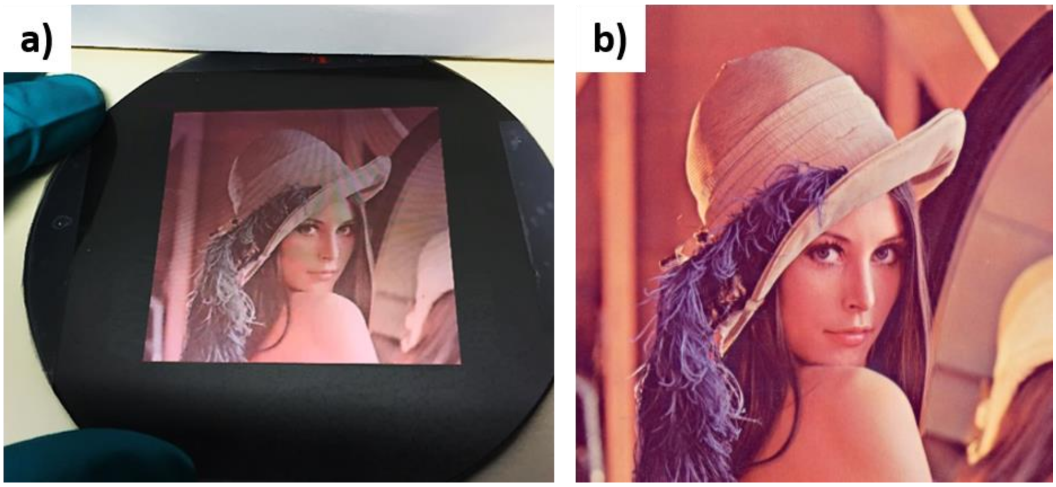

Figure 3.10. a) The image "Lena" made by the copper plasmonic RGB pixels. b) The standard Lenna image which is widely used to test the quality of colors in the field of image processing.

30µm*100 µm, which is smaller than the resolving power of human eyes. Because of the high reflectivity of each pixel, the image shows colors which are close to a real commercial display.

4. Nanofabrication of plasmonic materials

In the previous chapter, we roughly described several widely used nanofabrication technologies. Here, we will introduce more details about these technologies. Electron beam lithography (EBL) is one of the most widely used technologies for nanofabrication. It can reach extra high accuracy (~10 nm) [33]. However, EBL can only work for small samples since it is limited by the writing speed. Colloidal lithography (CL) is a nanofabrication technology which can be used for large area fabrication. This chapter will discuss both good and bad sides of these two technologies. Since we focus more on the large area fabrication technology, more information about CL will be presented.

4.1 Electron beam lithography (EBL)

The process of EBL is quite similar with laserlithography, the difference is EBL using the electron beam instead of the light beam [34]. First, the electron-sensitive resist needs to be coated on a substrate. Two different kinds of resists can be selected. One is positive resist which means the resist becomes dissolvable in the developer after exposing, another is negative resist which becomes hard to dissolve in the developer after exposing. The resist normally is coated by a spinner and the thickness of the resist can be adjusted by the spinning speed.

Second, the resist should be heated to change from the liquid state to the solid state. Depending on the kind of resist, different temperatures are required and also different heating times. Third, the substrate coated by resist is placed in a vacuum chamber and the electron beam is used with proper parameters to write the pattern on the substrate. Fourth, the sample is put into resist developer to remove the exposed part for positive resist or unexposed part for negative resist. A substrate with remaining resist pattern is achieved and will be used as a mask.

Then, metals and dielectrics are deposited on the patterned substrate. After removing the sample from the chamber, a resist remover is used to dissolve the remaining resist which is covered by the metals or dielectrics now. Then only the metals or dielectrics which are directly deposited on the substrate remain and form the plasmonic nanomaterial. Normally, the minimum size of the nanostructure is decided by the size of the electron beam, which can reach ~10 nm under perfect conditions [35]. In comparison with the colloidal lithography (CL), EBL can precisely pattern the plasmonic structure which is especially important to easily change the periodicity. However, the slow writing speed limits its use for large area patterning and EBL also needs to work in a vacuum environment which increases the cost and processing time a lot.

4.2 Colloidal lithography (CL)

Colloidal lithography (CL) is much cheaper and faster than EBL and utilizes nanoparticles as a mask instead of the electron beam processed resist [36]. After depositing metals or dielectrics and removing the nanoparticles, each nanoparticle can form one nanohole which is almost the same size as the nanoparticle. Because the nanoparticle mask can be made in a few minutes, it saves lots of time in comparison with EBL. In addition, CL doesn’t need a special machine to provide vacuum environment which saves lots of money as well. However, CL is limited by the structure of the nanoparticles, which can not be used for fabricating complex nanostructures. The periodicity of the nanoparticles is hard to precisely control compared with EBL [37]. We use the multilayer nanohole structure to generate colors for displays and it is made by CL. In this section, we will present more details of this technology.

The short range arrayed nanoholes in a gold film is one of the simplest structures prepared by colloidal lithography (CL). Both the size and periodicity of nanoholes can be roughly adjusted by using different colloidal solutions. Figure 4.1 shows the basic steps of fabrication of nanohole samples. The first step is adsorption of plastic particles on the glass substrate. Because the plastic particles have negative charges, the glass substrate needs positive charges to attract the particles. The positive charges can be introduced by putting the aluminum chlorohydrate (ACH) on the surface. The 5% concentration ACH solution should be dropped on a glass substrate first and left around 1 minute. Then, the sample should be rinsed and dried by nitrogen gas. Later, the colloidal solution is drop coated on the substrate followed by waiting another 2 minutes for the particle adsorption. To reinforce the stability of the plastic nanoparticles on the substrate, boiled ethylene glycol can be drenched on the substrate. The second step is deposition of different materials. 1 nm Cr should be deposited first because it is the adhesive layer between the glass substrate and the gold layer. Cr layer helps gold strongly attach on the glass substrate. Then, gold layer tens of nanometers in thickness is deposited and the deposition speed should be around 1 Å/sec. The last layer is 15 nm Al_2O_3 which is used to protect the gold surface for step 3. In step 3, the colloidal particles should be removed by a soft material like rubber or sponge. The Al_2O_3 layer protects the gold surface from being scratched by the soft material. After removing the particles, the last step is removing the Al_2O_3 layer. The Al_2O_3 layer can be removed in 30 mM NaOH solution. The standard way is to put the samples into the NaOH solution and wait around 1 hour. After drying, the nanoholes are formed.

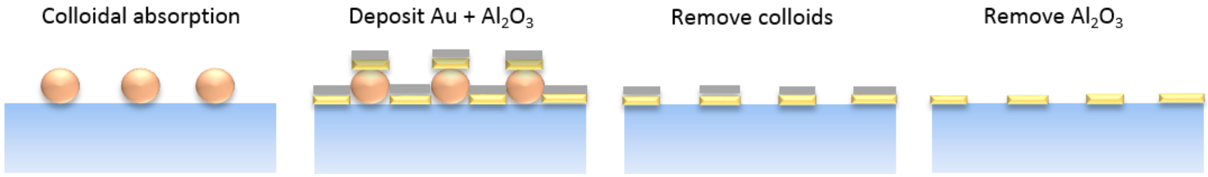

Figure 4.1. The process of colloidal lithography for short-range ordered nanoholes.

For the nanoholes structure, both the size and periodicity of nanoholes are totally decided by the particles in the colloidal solution. Particles with different sizes can be bought directly from a company. The distance between the neighboring particles is dependent on the amount of charges on the particles. In general, the smaller particles have less charges, so the distance between small particles is shorter than between large particles.

For size adjustment, different sizes of particles can be used to fabricate different nanoholes. However, one disadvantage of this method is that the size uniformity of particles is not good when the particle size is below 100 nm. Figure 4.2 shows different sizes of nanoholes which are made by colloidal lithography. It is quite clear that for the 58 nm nanoholes (top left), the size uniformity is quite bad. In fact, lots of nanoholes are larger than 60 nm and we estimated that the average size of nanoholes is 65 nm, not 58 nm as specified. Using quite small nanoparticles to get quite small nanoholes seems not to be an effective way. However, with increasing size of particles, the uniformity looks much better. The nanoholes with 105 nm diameter (bottom right) have much less size variation than 58 nm nanoholes.

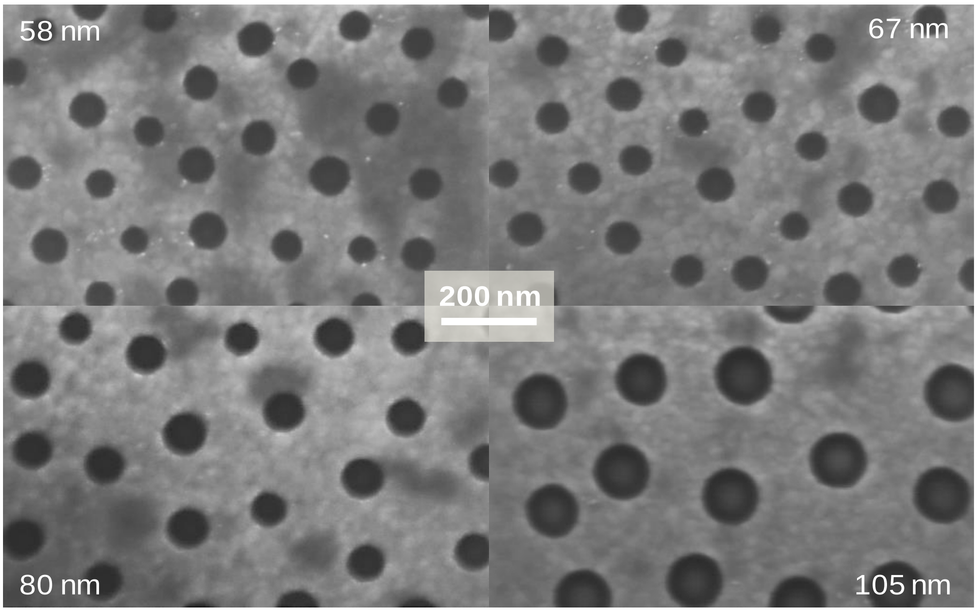

Figure 4.2. Different sizes nanoholes were made by different colloidal solutions.

Recently, one new method which can be used to fabricate uniform small nanoholes was invented [35]. It conserves the uniformity of large nanoholes and produces quite small nanoholes which are around 50

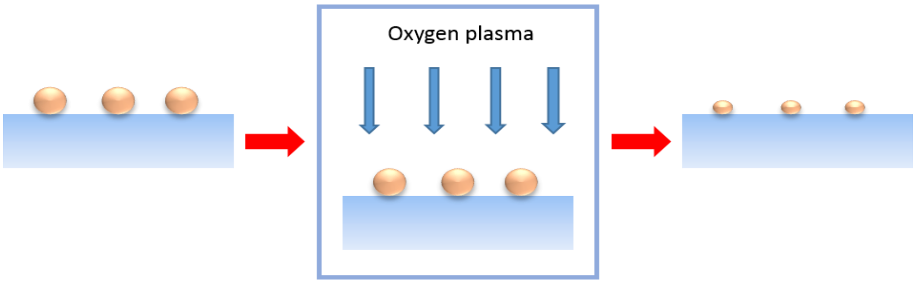

Figure 4.3. The process of shrinking the nanoparticles to get smaller nanoparticles.

nm. The method is that of shrinking the big particles by oxygen plasma after the particles are adsorbed on the substrate. After oxygen plasma shrinking, the size of particles becomes much smaller. Because the shrinking rate is quite uniform for each particle and the large particles have relatively uniform size, the shrunk small particles are also quite uniform [35].

The size of shrunken particles can be adjusted by the shrinking time. The average shrinking speed is around 1 nm/s. Fig. 4.3 shows the shrinking process. The initial size of particles is 158 nm. After the particles are absorbed on a substrate, they can be shrunk by oxygen plasma. The plasma power is 50 W, the pressure is 250 mTorr and gas speed is 80 sccm. Since the initial size of colloidal particles is 158 nm and the average shrinking speed is 1 nm/s, the shrinking time is around 108 s. One important point of using the oxygen plasma shrinking is that the shrinking speed could be not very stable because the shrinking speed is also related to the surface temperature of nanoparticles and the temperature of the nanoparticles will increase during the shrinking process [38]. To get more stable shrinking speed, the best option is cooling the sample after every 10 sec shrinking.

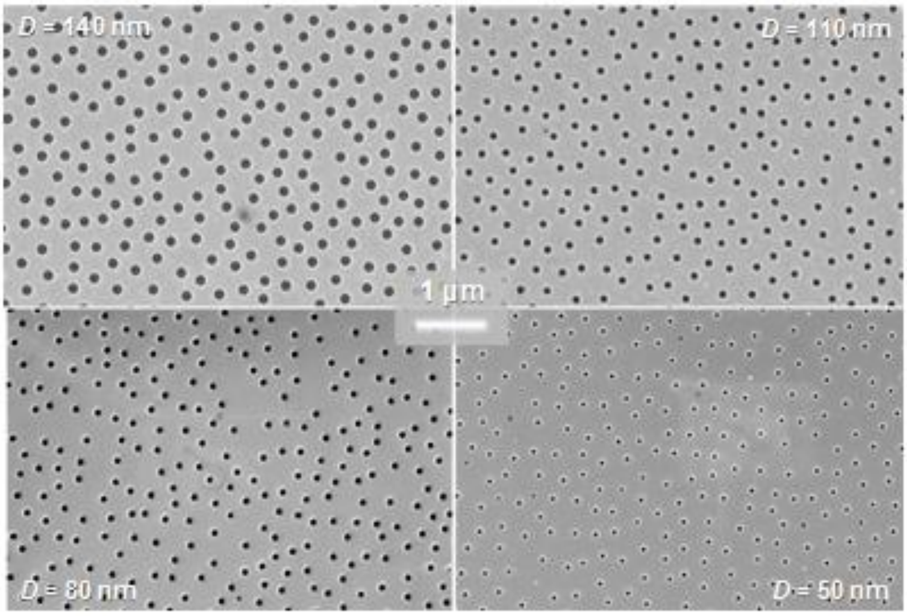

Figure 4.4. The SEM image includes four different nanoholes samples made by the same colloidal solution.

Figure 4.4 shows the nanoholes under SEM. It is obvious that these samples have almost the same uniformity. To compare with the samples directly made by small particles, the diameters of all the samples are analyzed. Fig. 4.5 shows the measured diameter histograms. For the samples which are made by particle shrinking, above 90% of nanoholes are in a variation of ±4 nm even for 50 nm nanoholes. However, for the nanoholes which are directly made by 58 nm particles, the size variation of the nanoholes is much larger.

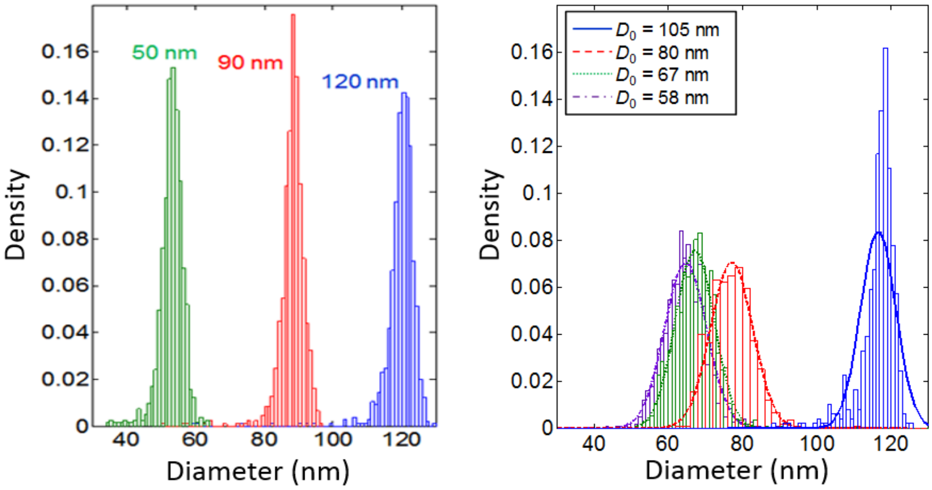

Figure 4.5. The histograms of measured diameters. The left figure is achieved by using the shrinking technology to get nanoholes. The right figure is achieved by directly using different sizes of PS particles to get nanoholes.

5. Implementing electrochromic polymers

In this thesis, I present a novel plasmonic electronic paper technology. The electronic paper includes two main parts where one is the color generator which has been described in Chapter 3. The other part is the color modulator which is made of electrochromic conjugated polymers (ECPs). I have already presented that the multilayer nanohole structure provides a high reflectivity and the thickness of the whole structure is only around hundreds of nanometers. I also presented that images made by plasmonic nanomaterials can have an extra high resolution. However, if I want to make a display based on the plasmonic nanostructures, I need to figure out a modulator which also has a thickness similar to the plasmonic materials. The reason is that the thickness of the modulator can limit the viewing angle of the display. Since the thickness of the liquid crystals is on the millimeter level which is much larger than the pixel size (hundred micrometers) [39], a small change in viewing angle can lead to a misalignment between the liquid crystal and the pixel. Thus, an electrochromic conjugated polymer is one good candidate since it can modulate the optical signal with hundreds of nanometers thickness and its soft texture perfectly matches with the plasmonic nanomaterials for a bendable display. In addition, the optical properties of the polymer can be maintained without applying voltages, which means it does not need energy to display static images [40]. Comparing with LCD and LED which need constant voltages when displaying, plasmonic electronic paper significantly reduces the energy consumption [41]. This chapter will first introduce the basic theory of the conjugated polymer and review several different kinds of electrochromic polymers. Then it will introduce the technology combining plasmonic materials and polymers. Last, I will discuss the optical properties of the novel plasmonic electronic paper.

5.1 Introduction of electrochromic conjugated polymers

Electrochromic polymers are characterized by a change in their optical properties upon reduction or oxidation, which is controlled by an electrical voltage. After discovering and characterizing the polyacetylene [53], the study of conjugated polymers rose rapidly. There are a lot of applications for conjugated polymer i.e. solar cells, organic light emitting device (OLEDs) and electrochromic devices. Normally, the conjugated polymer is p-type electroactive compounds since positive charges are generated upon oxidation. The positive charges of conjugated polymers can migrate along the chain by delocalized electrons in the alternating double bonds of the chain. These currents are responsible for the conductivity of the polymer [43], Fig. 5.1 shows how the system works. During the oxidation, the polymer has a local distortion of the chain in the proximity of the charge, then it is pictured as a quinoid-like structure in which single bonds assume double bonding character [44].

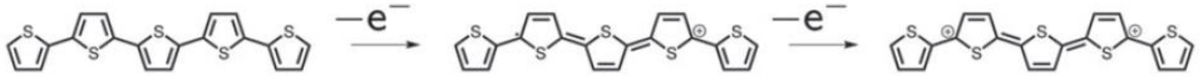

Figure 5.1. The process of oxidation of a conjugated polymer.

To further analyze the physical model of the conjugated polymer, I introduce the band diagrams to explain the optical properties. Depending on the doping levels, the conjugated polymers have polaron states (low doping) or bipolaronic states (high doping) respectively. In conjugated polymers with a ground state (Fig. 5.2a), the positively charged states are called bipolaron states, which are localized inside the band gap of the polymer (Fig. 5.2b) [45]. For the bipolaronic state polymer, there are two sub-gap (low energy) transitions from the valence band to the localized (E_{b1} and E_{b2}) bipolaronic states.

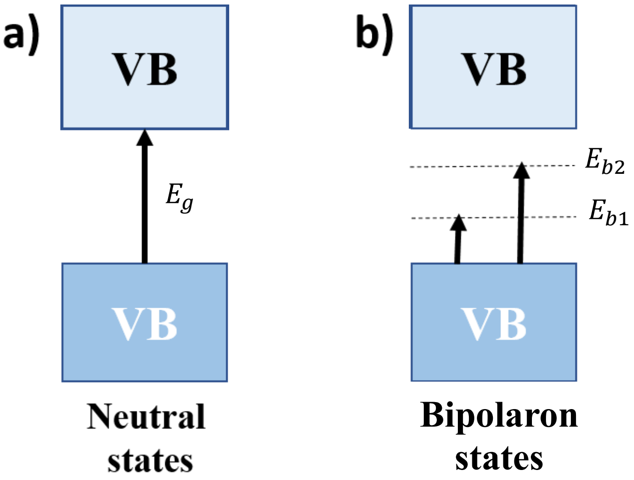

Figure 5.2. The neutral and bipolaron states of the conjugated polymer.

The optical absorption band in the reduced neutral conjugated polymer is determined by a $\pi - \pi^*$ transition through the band gap [46]. Thus, the energy levels of the localized bipolarons dominate the optical properties since the observed color depends upon the bandgap of the polymer. Thin films of polymers with $E_g > 3$ eV are colorless since it is out of the visible color range. However, they can become colorful if their doped forms absorb visible light. In contrast, those with lower band gaps $E_g <$ 1.5 eV show colored reduced forms and have a weak colored or colorless doped form. After the doping, the absorption shifts to the NIR region which cannot be seen by human eyes. In next section, I will review several electrochromic conjugated polymers, such as PEDOT. PEDOT has "bright state" in its oxidized state and polypyrrole (ppy) has "black state" in its oxidized state [47] [48]. I will also discuss their optical properties.

5.11 Poly [3, 4-(ethylenedioxy) thiophene] (PEDOT)

PEDOT possesses a relatively stable and highly transmissive sky-blue oxidized state, which is suitable for a polymer-based electrochromic device (ECD) [49]. The absorption band of reduced PEDOT lies in the near infrared region which leads to a dark blue color. PEDOT has a fairly high optical contrast, good mechanical properties, low switching times and low cost [50]. Meanwhile, PEDOT is a good electrical conductor which keeps its conductivity in both reduced and oxidized states [51]. This property is hard to find in other conjugated polymers. In our devices, I use PEDOT to modulate the optical properties of the copper-based plasmonic samples, as will be discussed later.

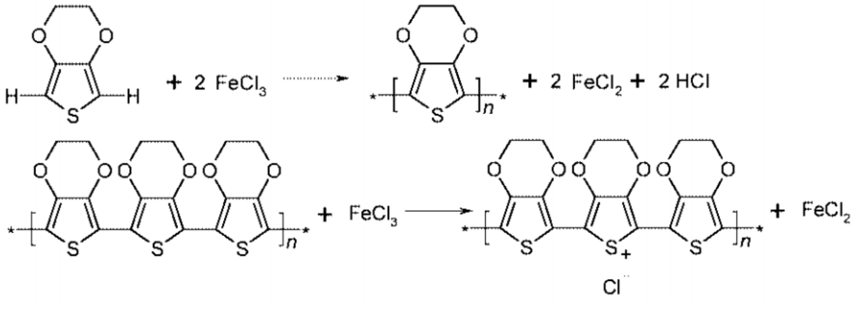

Figure 5.3. The chemical reaction of polymerization of the EDOT monomer.

The chemical reaction of polymerization of the EDOT (3, 4-(ethylenedioxy) thiophene) monomer is shown in Figure 5.3. One can use the $FeCl_3$ as the oxidant and coat the PEDOT on the copper-based plasmonic material by a vacuum vapor phase polymerization [52]. Vacuum vapor phase (VVP) polymerization is suitable for coating large areas and it can be used to coat dielectrics. First, an oxidant solution containing iron chloride hexahydrate ($FeCl_3$) is coated by a spinner. Normally the substrate is made of chemically resistant materials since the $FeCl_3$ solution is a fairly strong Lewis acid. Then, the EDOT and the coated substrate are put into a chamber. After pumping the chamber to create a vacuum environment, the EDOT is heated to around 60 °C. The EDOT will be evaporated inside the chamber and start to be polymerized and deposited on the substrate surface. The thickness of the coated PEDOT is controlled by the reaction time.

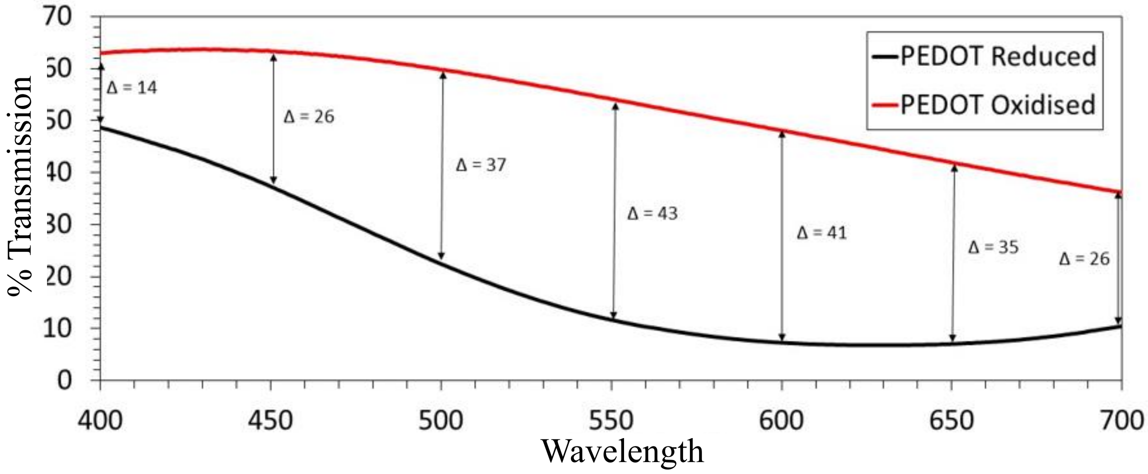

Figure 5.4. The optical signals change in different states.

Screen printing is another technology to coat PEDOT on plasmonic samples [54]. Poly(3,4-(ethylenedioxy) thiophene)polystyrene sulfonate (PEDOT:PSS) as a commercial PEDOT can be bought directly. PEDOT:PSS is a mixture of PEDOT and sodium polystyrene sulfonate. PEDOT:PSS is used as a transparent, conductive polymer with high ductility and it can dissolve in water to form gelated particles. PEDOT:PSS can be prepared as a highly viscous paste in propanediol, which can be used for screen printing. Screen printing is a printing technique which is using a mesh to transfer ink onto a substrate. In my case, the thickness of PEDOT:PSS can be adjusted by the thickness of the mesh or the polymer concentration in the solution.

Concerning the optical properties of the PEDOT, Figure 5.4 shows the visible spectrum of PEDOT in different states. It is obvious the PEDOT has relatively high optical contrast (~40%) for the green (520nm to 560nm) and red color (620nm to 740nm). However, because of the contrast in blue (450nm to 490nm) is less than red and green, it is hard to get a completely black state and some blue color remains. Even though I can adjust the contrast by depositing PEDOT with different thicknesses for modulating different colors, precisely controlling different thicknesses in different areas of one substrate is still a big challenge for both VVP and screen printing technologies, which is important for electronic paper application. More details about modulation of PEDOT-plasmonic materials will be discussed later. In the next section, I will discuss another kind of conjugated polymer which is polypyrrole (ppy).

5.12 Polypyrrole (PPy)

Polypyrrole (PPy) is by far the most extensively studied polymer in this research area because of its low oxidation potential, water solubility and the low cost of its monomer [55]. PPy is in black or bright modes for the oxidized or reduced states respectively, which is the opposite of PEDOT. Thus, PPy and PEDOT could be used as the cathode and anode sides in an electrochemistry system to modulate the optical signals. For the synthesis of PPy, electrochemical polymerization is a frequently used technology because it requires a small amount of monomer and it provides an effective platform that allows investigating the growing process of the polymer by electrochemistry and spectroscopy [56]. Figure 5.5 shows a system that contains combined electrochemical and spectroscopic systems. The system uses Ag/AgCl as the reference and Pt as the counter electrode which is connected to the potentiostat to control the voltage and measure the current. Meanwhile, the light source is coupled to an optical fiber and the spectrum can be measured by a fiber-coupled spectrometer. Since copper is an easily oxidized metal it will be etched during electrochemical deposition and thus I have to use the gold containing color generators. The solution for deposition is a mixture of NaDBS and pyrrole. Before electrochemical deposition, I install the gold color generator in a flow cell which contains the reference (Pt) and counter(Ag/AgCl), then inject the mixture. The polypyrrole will be deposited by applying +0.57 V versus Ag/AgCl and the growth rate is around 40 nm/min. This process is monitored by the plasmonic sensing with high resolution [57] and the thickness can be accurately controlled by the current.

The mechanism of polymerization of pyrrole is shown in Fig. 5.6. The oxidized monomers bond together to form a long chain. It should be noticed that DBS is also doped into PPy during the electrochemical deposition. In fact, PPy does not consist of linear chains but is heavily crosslinked [58] (Fig. 5.6). This crosslink traps the DBS within the PPy matrix. For the optical properties, PPy has an even weaker contrast for blue color. The optical property of the polymerized sample is modulated by electrochemistry [59]. One only needs to exchange the solution from the mixture with pyrrole to only NaDBS. About the optical property modulation, it will be discussed in the next section.

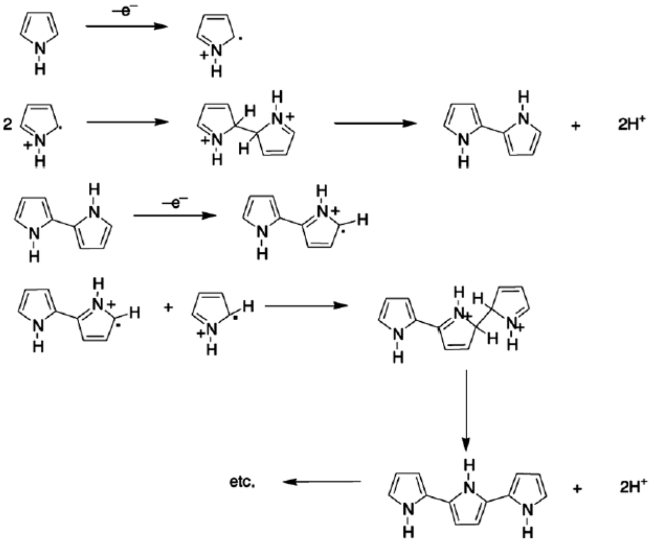

Figure 5.6. Polymerizing pyrrole to form PPy. The image is from reference [58].

5.2 Electrochemical modulation

For both PEDOT and PPy based plasmonic electronic papers, electrochemical technology is used to modulate the reflection. The color is easily switched “on” or “off” by applying maximum ±1 V. The whole system can be flexible if a soft substrate (plastic) and a suitable counter/reference (thin ITO, polymer, carbon paste, etc.) are used [60]. Fig 5.7 shows a system consisting of PPy and gold based plasmonic color generators, and the reflection is electrochemically controlled. Since gold is one of the best conductors and it has a strong chemical resistance, a thin (~20 nm) gold layer can work as the top layer of the color generator and also as a working electrode which controls the "on" or "off" state of the PPy. Then color is switched "on" by applying around ~-1 V (vs Ag/AgCl) to reduce the conductive polymer to its neutral state, leading to strongly reduced absorption [61]. As a result, the reflections from the RGB samples can be modulated with a high contrast.

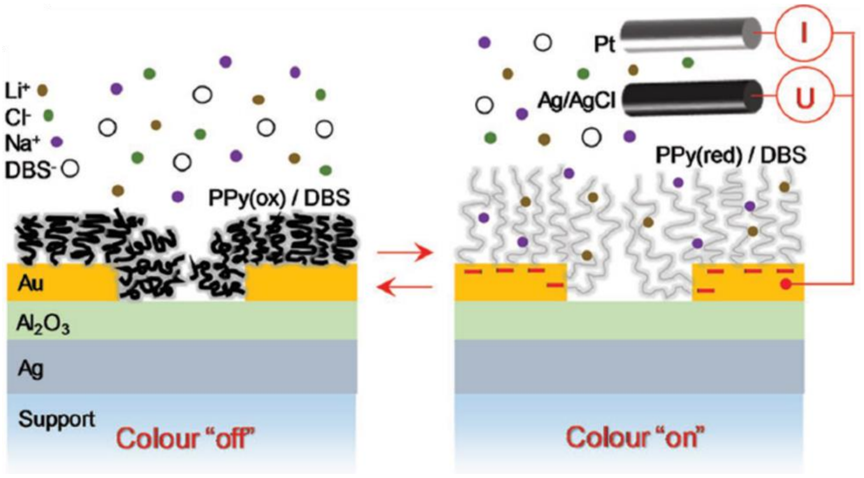

Figure 5.7. Electrochemical control of "on" and "off" states of color generators.

The spectra of RGB samples in "on" or "off" state and the sensitive region of the human eye under well-lit conditions are shown in Figure 5.8. The reflections from the RGB samples could be modulated with high contrast. The spectra are slightly shifted compared with the initial colors since the structures now are in contact with polymer and electrolyte, but the colors appear very similar. The sensitive region is defined as the wavelength interval where the luminosity function for photopic vision is > 5% of its maximum.

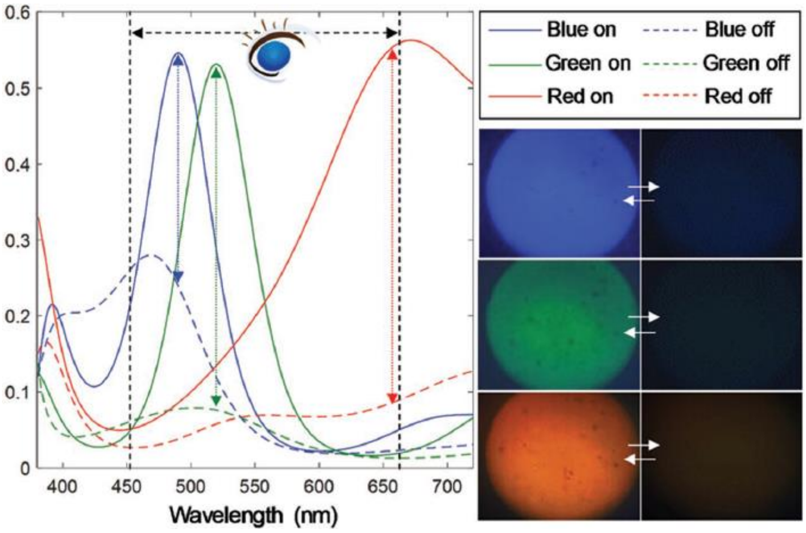

Figure 5.8. Reflection spectra and images of RGB samples in on/off states.

Comparing with gold-PPy, PEDOT-copper based plasmonic electronic paper is much cheaper with better optical contrast, especially for blue color. Since copper is not as chemically stable as gold, it can not be directly used as a working electrode. Thus, I cannot use electrochemical technology to deposit PPy on copper. One needs to coat a protection layer on the copper surface to avoid etching due to the electrolyte solution. In our case, I first deposit 20 nm Al_2O_3 after the colloidal lithography and then an

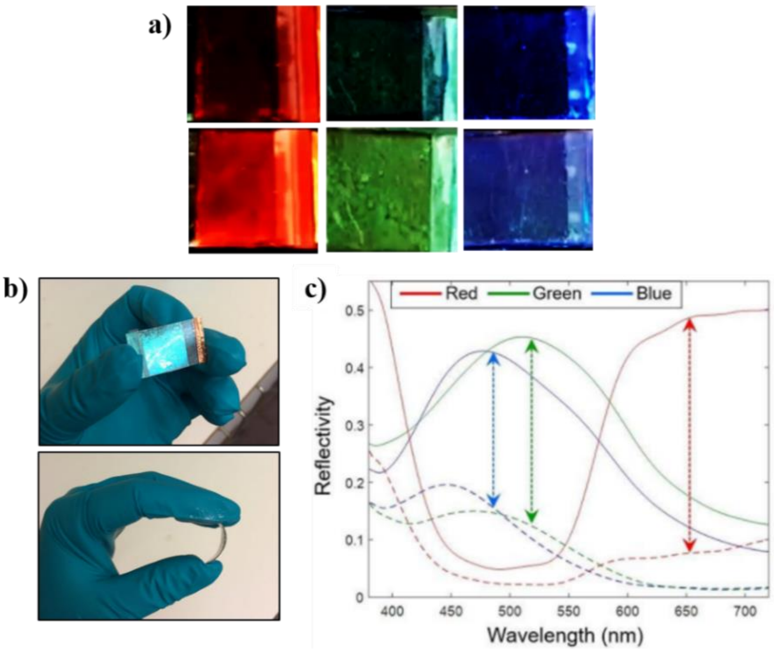

Figure 5.9. a) Pictures showing "on" and "off" states of RGB samples. b) The whole system is bendable. c) Reflection spectra of RGB samples in "on" or "off" state.

additional 100 nm SiO_2 to cover the nanoholes and defects of the Al_2O_3 layer. PEDOT is perfectly matched with the copper-based plasmonic samples. It can be used as a working electrode since it is a conductor in both reduced and oxidized states and it also works as an optical modulator. I print PEDOT on the plasmonic color generator by screen printing and the “on” and “off” states for RGB samples is shown in Fig. 5.9. In this system, I use thin ITO (25 nm) as the counter and PET as the substrate, so the whole system is bendable (Fig. 5.9b).

In conclusion, these reflective color displays should be especially useful for large-area energy-efficient electronic readers and posters, which are also simple to fold and transport. For the PEDOT- copper based electronic paper, the cost of the materials is low and commercially available. More details about the plasmonic electronic paper will be discussed in the next chapter.

6. Discussion and future outlook

In this chapter, more details about the plasmonic electronic paper will be discussed, which include the color analysis, energy consumption and response time. We compare the properties of plasmonic electronic paper with other similar devices and also discuss the merits and drawbacks. Last, the future outlook of electronic paper is presented. We will briefly introduce some future plans to improve our devices.

6.1 Discussion on plasmonic electronic paper

First, we introduce some background about the characterization of color from displays. The CIE color space is used to define the quantitative links between physically measured wavelengths and physiologically perceived colors in human eyes [62]. The human eyes have three kinds of cone cells to sense colors, which are sensitive in 420-440 nm as the short wavelength region, 530-540 nm as the middle wavelength region and 560-580 nm as the long wavelength region. Based on the three regions, people set up a CIE XYZ color space encompassing all color sensations that an average person can

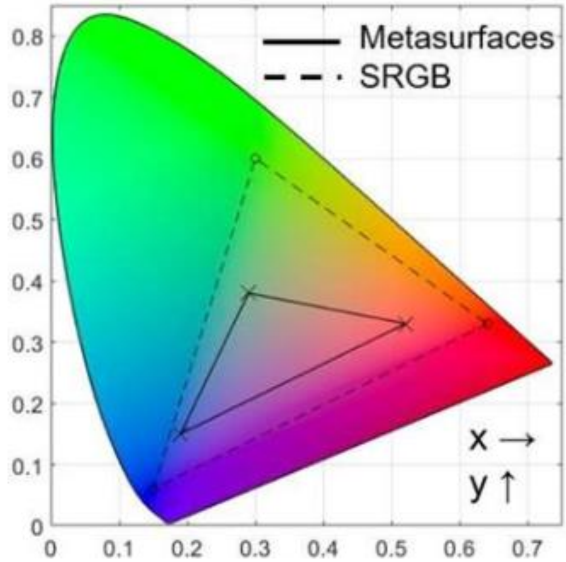

Fig. 6.1 Chromatic calculation for the RGB copper based on the plasmonic metasurface.

experience. CIE color space is used as a standard reference to estimate the quality of color generators and the occupied area of the CIE color space represents the color gamut. Fig. 6.1 shows the color gamut of the copper-based plasmonic color generators. All colors inside of the triangle can be generated by mixing three primary colors represented by the points in the chromaticity diagram. The color range of the RGB metasurfaces are according to the CIE “standard observer” functions from 1931 [62]. The CIE’s color matching functions $x(\lambda)$, $y(\lambda)$ and $z(\lambda)$ denotes the chromatic response of the observer. We first calculate the tristimulus values based on the color functions:

$$\boldsymbol{Y} = \int_{380}^{780} \boldsymbol{R}(\lambda)y(\lambda)d\lambda \tag{5.11a}$$

$$\boldsymbol{Y} = \int_{380}^{780} \boldsymbol{R}(\lambda)y(\lambda)d\lambda \tag{5.11b}$$

$$\boldsymbol{Z} = \int_{380}^{780} \boldsymbol{R}(\lambda)z(\lambda)d\lambda \tag{5.11c}$$

where R is the reflectivity of the RGB samples and the integral range 380 to 780 nm represents the whole visible region in nm. After normalizing, the CIE coordinates become:

$$\overline{\boldsymbol{x}} = \frac{\boldsymbol{X}}{\boldsymbol{X}+\boldsymbol{Y}+\boldsymbol{Z}} \tag{5.12a}$$

$$\overline{\boldsymbol{y}} = \frac{\boldsymbol{Y}}{\boldsymbol{X}+\boldsymbol{Y}+\boldsymbol{Z}} \tag{5.12b}$$

$$\overline{\boldsymbol{z}} = \frac{\boldsymbol{Z}}{\boldsymbol{X}+\boldsymbol{Y}+\boldsymbol{Z}} \tag{5.12c}$$

For the copper based color generator, the coordinate of R is (0.52,0.33), G is (0.28,0.38) and B is (0.19,0.15).

Second, I present the energy consumption of the plasmonic electronic paper. Similar to the EPD displays, plasmonic electronic paper does not need to keep on supplying voltages or currents to maintain the colors for the display under the right circumstances. Further, the voltages for switching the color are much lower than EPD [63], which leads to much lower energy consumption. Considering the stability of the electrochemical system, the ideal voltages of PPy for switching the colors fully on were -0.9, -1.0. and -0.8 V vs Ag/AgCl for RGB respectively. We compare the energy consumption to emissive displays (LED) and EPD, as is shown in Fig. 6.2. The power densities correspond the energy cosumption of displays, and our plasmonic electronic paper is more than two orders of magnitude lower than LED and one order lower than EPD [2].

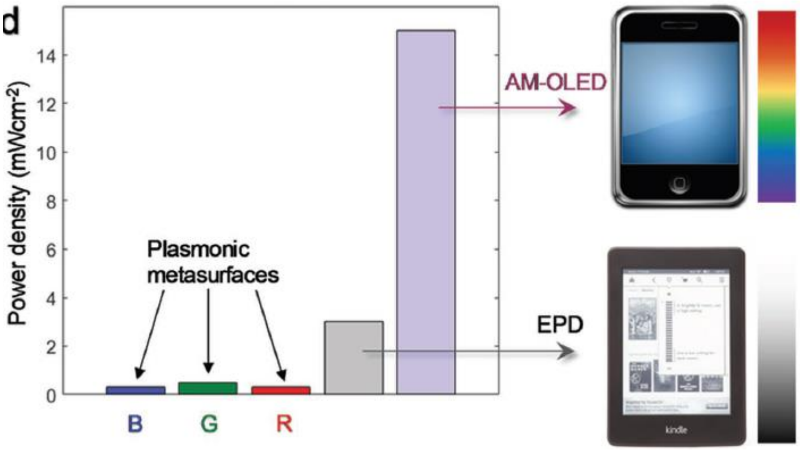

Fig. 6.2 The power density of the PPy-gold based plasmonic electronic paper for the RGB colors compared with average power use for black and white electrophoretic displays and active-matrix organic light-emitting diode (AM-OLED) displays.

Last, about the response time, the electronic paper takes less than 1 s to turn the colors on or off. In the future it can be used to display images or texts but can not display videos. In Fig. 6.3a, the current trace shows switching the metasurfaces every ~10 s and also the reflection variation together with the current. The thickness of the PPy is around 200 nm. It is obvious that the reflection is stable after ~1 s which is

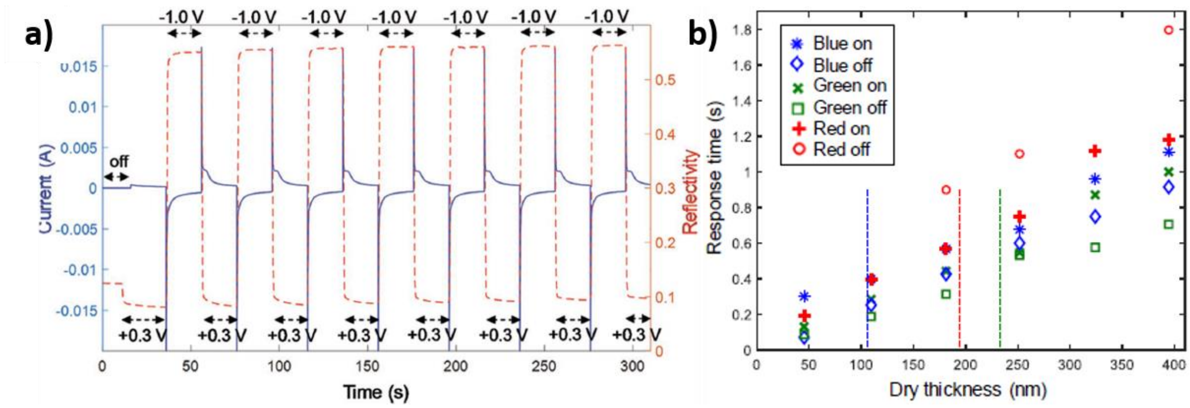

Fig. 6.3 a) Switching dynamics (for a red sample) showing current (electrode area 176 mm^2) and reflectivity at 660 nm versus time as the voltage is reversed. b) Response times versus colors and PPy thickness.

shorter than the stable time of the electric current. More details about the shifting time for different RGB colors and thickness of the polymer are shown in Fig 6.3b.

6.2 Future outlook

In this thesis, I have presented a novel electronic paper consisting of electrochromic polymers and plasmonic color generators. I started with introducing the commercial displays like CCRT, LCD, LED, etc. and discussed their limitations and merits. Then, the theoretic part of plasmonics is presented in chapter 2, which provides the basic knowledge to understand the optical properties of plasmonic materials. In chapter 3, several plasmonic color generators are discussed including their structure, size and the elements used. My color generators which have metal-insulator-metal structures are discussed later. After analyzing the optical properties of my color generators, the fabrication technologies are presented in chapter 4 and I also discuss how to adjust the diameter and periodicity of the nanoholes. In chapter 5, I start to introduce and analyze the optical properties of the electrochromic polymers. Then the optical properties of the plasmonic electronic paper, which is the combination of the polymers and color generators, are shown. Last, I discuss several advantages of the novel electronic paper.

In the future, the most challenging next step is to implement transistor arrays with the conductive polymers [54] which can individually control each pixel of the plasmonic electronic paper. This step is a basic requirement for a commercial display. Then, the optical contrast of the electrochromic polymer should also be improved since it is still smaller than for EPD now. Further, the plasmonic electronic paper can not display videos since it is limited by the shifting time (~1 s) of the polymers. I want to decrease the shifting time to the tens of ms level which is good enough for video display. One method could be combining the polymer blinds [66] with my color generators since the shifting speed of the polymer blinds can reach to ms level. Last, I want to improve the reflection of the plasmonic color generators by combining them with fluorescent materials such as quantum dots [64]. The fluorescent materials can transfer the high energy photons to low energy photons. For example, they can transfer green light into red light, so if I can put them into the electrolyte, they can increase the amount of reflected red light.

Plasmonic electronic paper provides a colorful, bendable and low energy consumption display technology, which overcomes the limitations of EPD (no colors) and RLCD (low reflectivity and not bendable). It gives excellent visibility in sunshine and should be healthier for the human eyes compared to emissive displays [65]. It is very exciting for me to look forward to the development of this technology.

Acknowledgements

I would like to express my sincere gratitude to Prof. Andreas B. Dahlin, for employing me to start my PHD life in Chalmers. As the supervisor of my project, he always supports and encourages me during the research. He patiently teaches me and cares for my life like a brother. It is very lucky to work for him. I would also like to thank my co-supervisor, Prof. Edwin Jager. Even he is not working in Chalmers instead of linkoping university, he is still carefully teaching and supporting me useful information. I learned the deposition polymer technologies directly from him, which is a quite important part for my project. Thanks a lot for my department leader Anders Palmqvist and ph.d defence opponent Prof. Asger Mortensen. They help and discuss a lot for my phd thesis.

Many thanks as well to my colleagues Gustav Emilsson, who helps me to finish lots of chemistry experiments and we always discuss plans in the daily research. Lei Shao is also one of the best advisers, I always can get some new ideas from our discussion. Yurui wang as a postdoc teaches me lots of theoretical knowledge and software technologies. Martin Wersäll shared the office with me, he always help me both on research and daily life. He lets me know lots of Sweden cultures and friendly invites me to join some activities. Ruggero Verre and Srdjan Acimovic who are experienced researchers, they always helps me fabrication samples and gives lots of useful advises. My new colleages Bita Malekian, Zeynep Adali and Gustav Ferrand-Drake Del Castillo help me a lot in my daily life. We have lots of good memory together. I appricate that I can work in so lovely group.

Then, I would like to thank two postdoc friends, Zhaoyang Zhang and Lihui Liu. Both of them are from Jie Sun group. We always play together and discuss academic problems during the lunch time. They have rich physics and electrochemistry knowledge, they always help me to find useful experimental materials and equipments, encourage me when I have troubles.

To my family: First, I want to say I am the luckiest man in the world to get married with my wife Zi Yang. She always encourages me and warms my heart. She is one of the biggest source energies to push me working hard. Now, we have a newborn son Leon, I am living in happiness

every day. I also want to thank my parents to support me working abroad. They are always care of my health and research by internet communication software.

Finally, I want to thank my Ph.D. funder Strategic Research and Chalmers Nanoscience and Nanotechnology Area of Advance to give me such a chance to be as a Ph.D. student. I also want to thank Sweden, which is an equal, free and mercy country! Friendly people, nice environment and good English pronunciation. Hopefully the weather could be better in the future.

^.^

Kunli xiong

Göteborg, Sweden

October 13th,2017.

Reference

1. J. A. Castellano. Handbook of Display Technology. *Califormia* (**1992**).
2. M. R.Fernández, E. Z. Casanova and I. G. Alonso. Review of Display Technologies Focusing on Power Consumption Stochastic sensors inspired by biology. *Sustainability* (**2015**), 7, 10854-10875.
3. R.Williams. Domains in Liquid Crystals. *J. Chem. Phy* (**1963**), 39, 384.
4. N. Holonyak, and S. F. Bevacqua. Coherent (visible) light emission from a gallium phosphide junction. *Applied Physics Letters* (**1962**), 1, 82.
5. B. W. D'Andrade and S. R. Forrest. White Organic Light-Emitting Devices for Solid-State Lighting. *Advanced Materials* (**2004**), 16, 18.
6. K. Xiong, G. Emisson, A. Maziz, X. Yang, L, Shao, E. W.H. Jager & A. B. Dahli., Plasmonic Metasurfaces with Conjugated Polymers for Flexible Electronic Paper in Color. *Advanced Materials* (**2016**), 28, 9956-9960.
7. J. D. Jackson. Classical Electrodynamics 3rd edition. *New York* (**1999**).
8. P. Drud. Zur Elektronentheorie der Metalle. *Annalen der physic* 306 (**1900**), 566.
9. C. F. Bohren, and D. R. Huffman. Absorption and scattering of light by small particles first edition. *New York* (**1998**).
10. M. Abramowitz, I. Stegun. Handbook of Mathematical functions with Formulas, Graphs and Mathematical Tables. *New York* (**1964**).
11. J. M. Pitarke, V. M. Silkin, E. V. Chulkov and P M Echenique. Theory of surface plasmons and surface-plasmon polaritons. *Rep. Prog. Phys* (**2007**), 70, 1–87.
12. M.P. Jonsson, A.B. Dahlin, P. Jönsson, F. Höök. Nanoplasmonic biosensing with focus on short-range ordered nanoholes in thin metal films. *Biointerphases* (**2008**), 3 (3), 30-40.
13. R. Kekesi, D. Meneses-Rodriguez, F. Garcia-Perez, M. U. Gonzalez, A. Garcia-Martín, A. Cebollada and G. Armelles. The effect of holes in the dispersion relation of propagative surface plasmon modes of nanoperforated semitransparent metallic films. *Journal of Applied Physics* (**2014**), 116, 134306.

14. K. Xiong, G. Emilsson, A. B. Dahlin. Biosensing using plasmonic nanohole arrays with small, homogenous and tunable aperture diameters. *Analyst* (**2016**), 141 (12), 3830-3810.
15. T. Park, N. Mirin, J. B. Lassiter, C. L. Nehl, N. J. Halas, and P. Nordlander. Optical Properties of a Nanosized Hole in a Thin Metallic Film. *ACS Nano* (**2008**), 2(1), 25-32.
16. A. B. Dahlin, M. Mapar, K. L. Xiong, F. Mazzotta, F. Hook and T. Sannomiya. Plasmonic nanopores in metal-insulator-metal films. *Adv. Opt. Mater* **(2014**), 2, 556–564.
17. T. Sannomiya, O. Scholder, K. Jefimovs, C. Hafner and A. B. Dahlin. Investigation of plasmon resonances in metal films with nanohole arrays for biosensing applications. *Small* (**2011**), 7, 1653–1663.
18. J. Junesch, T. Sannomiya and A. B. Dahlin. Optical properties of nanohole arrays in metal-dielectric double films prepared by mask-on-metal colloidal lithography. *ACS Nano* (**2012**), 6, 10405–10415.
19. I. Freeston, N. Meeks, M. Sax, C. Higgitt. The Lycurgus Cup- A Roman Nanotechnology. *Gold Bulletin* (**2007**), 404.
20. W. H. Burnham. Stained Glass Windows. *Design* (**1946**), 4, 48.
21. P. Colomban. The use of metal nanoparticles to produce yellow, red and iridescent colour, from bronze age to present times in lustre pottery and glass: solid state chemistry, spectroscopy and nanostructure. *J. Nano Res*. (**2009**), 8, 109–132.
22. F. A. Stevie, L. A. Giannuzzi and B. I. Prenitzer. Introducion to Focused Ion Beams. *Orlando* (**2004**).
23. P. Hanarp, D. S Sutherland, J. Gold, B. Kasemo. Control of nanoparticle film structure for colloidal lithography. *Colloids and Surfaces A: Physicochem* (**2003**), 214, 23 -36.
24. Ye, M. et al. Angle-insensitive plasmonic color filters with randomly distributed silver nanodisks. *Opt. Lett* (**2015**), 40, 4979–4982.
25. C. W. Hsu, et al. Transparent displays enabled by resonant nanoparticle scattering. *Nat. Commun* (**2014**), 5, 3152

26. J. B. Khurgin, A. Boltasseva. Reflecting upon the Losses in Plasmonics and Metamaterials. *MRS Bull* (**2012**), 37, 768–779.
27. J. M. McMahon, G. C.Schatz and S. K. Gray. Plasmonics in the Ultraviolet with the Poor Metals Al, Ga, In, Sn, Tl, Pb, and Bi. *Phys. Chem. Chem. Phys.* (**2013**), 15, 5415–5423.
28. M. W. Knight, N. S. king, L. Liu, H. O. Everitt, P. Nordlander, and N. J. Halas. Aluminum for plasmonics. *ACS Nano.* (**2013**), 8, 834-840.
29. B. Auguie and W. L. Barnes. Collective Resonances in Gold Nanoparticle Arrays. Rhy. Rev. Let. (**2008**), 101, 143902.
30. H. Lochbihler. Colored images generated by metallic sub-wavelength gratings. *Opt. Express* (**2009**),17, 12189–12196.
31. L. Duempelmann, et al. Four-fold color filter based on plasmonic phase retarder. ACS Photonics 3, 190–196 (**2016**).
32. K. Kumar, et al. Printing colour at the optical diffraction limit. *Nat. Nanotechnol* (**2012**), 7, 557–561.
33. J. Fujita, Y. Ohnishi, Y. Ochiai, and S. Matsui. Ultrahigh resolutuion of calixarene negative resist in electron beam lithography. *Appl. Phys. Lett.* (**1996**), 68, 1297.
34. M. A. McCord, M. J. Rooks. SPIE Handbook of Microlithography, Micromachining and Microfabrication. *Institution Of Engineering And Technology, USA* (**1997**).
35. M. P. Seah, W. A. Dench. Quantitative electron spectroscopy of surfaces: A standard data base for electron inelastic mean free paths in solids. *Surface And Interface Analysis* (**1979**), 1, 1.
36. F. Burmeister, et al. From Mesoscopic to Nanoscopic Surface Structures: Lithography with Colloid Monolayers. *Advanced Materials* (**1998**), 10, 495-49.
37. J. Wang, et al. Wet Etching-Assisted Colloidal Lithography: A General Strategy Toward Naanodisk and Nanohole Arrays on Arbitrary Substrates. *Appl. Mater. Interfaces* (**2014**), 6, 9207-9213.

38. Q. Li, X. Han, J. Hou, J. Yin, S. Jiang, C. Lu. Patterning Poly (dimethylsiloxane) Microspheres via Combination of Oxygen Plasma Exposure and Solvent Treatment. *J. Phys. Chem. B* (**2015**), 119, 13450−13461.

39. D. Franklin, R. Frank, S. Wu and D. Chanda. Actively addressed sigle pixel full-colour plasmonic display. *Nat. Commun* (**2017**), 10, 1038.'

40. H. Shin, et al. Color Combination of Conductive Polymers for Black Electrochromism. *Mater. Interfaces* (**2012**), 4, 185-191.

41. Y. Ukai. TFT-LCDs as Future Leading Role in FPD. *SID* (2013), 44, 28-31.

42. A. M. Saxman, R. Liepins, M. Aldissi. Polyacetylene: Its synthesis, doping and structure. Prog. Polym. *Sci.* (**1985**), 11, 57-89.

43. L. Beverina, G. A. Pagani and M. Sassi. Multichromophoric electrochromic polymers: colour tuning of conjugated polymers through the side chain functionalization approach. *Chem. Commun*. (**2014**), 50, 5413.

44. J. L. Bredas and G. B. Street, Polarons. Bipolarons and solitons in Conducting Polymers. *Acc. Chem. Res.* (**1985**), 18, 309-315.

45. A. J. Heeger, S. Kivelson, J. R. Schrieffer, W.-P. Su. Solitons in conducting polymers. *Rev. Mod. Phys.* (**1988**), 60, 781–850.

46. T. A. Skotheim, J. Reynolds. Handbook of Conducting Polymers Fourth Edition. *CRC Press* (**2007**).

47. D. Hohnholz, A. G. MacDiarmid, D. M. Sarno and W. E. Jones. Uniform thin films of poly-3,4-ethylenedioxythiophene (PEDOT) prepared by in-situ depostition. *Chem. Commun.* (**2001**), 0, 2444-2445.

48. P. Camurlu. Polypyrrole derivatives for electrochromic applications. *RSC Adv* (**2014**),4, 55832.

49. J. C. Gustafsson-Carlberg, O. Ingana¨s, M. R. Andersson, C. Booth, A. Azens and C. G. Granqvist. Tuning the bandgap for polymeric smart windows and displays. *Electrochim. Acta* (**1995**), 40, 2233–2235.

50. J. Jensen, M. Hösel, A. L. Dyer, and F. C. Krebs. Development and manufacture of polymer-based electrochromic Devices. *Adv, Funct, Mater* (**2015**), 25, 2073-2090.

51. A. Malti, et al. Freestanding electrochromic paper. *J. Mater. Chem. C* (**2016),** 4, 9680-9686.
52. R. Brooke, et al. Effect of oxidant on the performance of conductive polymer films prepared by vacuum vapor phase polymerization for smart window applications. *Smart mater. Struct.* (2015), 24, 035016.
53. H. Shirakwa, et al. Synthesis of electrically conducting organic polymers: halogen derivatives of polyacetylene, $(CH)_x$. *J. Chem. Soc., Chem. Commun.* (**1977**), 578-580.
54. P. A. Ersman, J. Kawahara, M. Berggren. Printed passive matrix addressed electrochromic displays. *Org. Electron*. (**2013**), 14, 3371-3378.
55. L.-X. Wang, X.-G. Li and Y.-L. Yang. Preparation, properties and applications of polyprroles. *React. Funct. Polym*. (**2001**), 47, 125.
56. A. B. Dahlin, T. Sannomiya, R. Zahn, G. Ga. Sotiriou and J. Vörös. Electrochemical Crystallization of Plasmonic Nanostructures. *Nano Lett.* (**2011**), 11, 1337-1343.
57. A. B. Dahlin, et al. High-Resolution Microspectroscopy of Plasmonic Nanostructures for Miniaturized Biosensing. *Anal. Chem.* (**2009**), 81, 6572-6580.
58. E. M. Genies and G. Bidan. Spectroelectrochemical Study of Polypyrrole Films. *J. Electroanal. Chem.* (**1983**), 149, 101-113.
59. T. Sannomiya, H. Dermutz, C. Hafner, J. Vörös. Electrochemistry on a localized surface plasmon resonance sensor. *Langmuir* (**2010**), 26, 7619-7626.
60. S.-I. Na, S.-S. Kim, J. Jo and D.-Y. Kim. Efficient and Flexible ITO-Free Organic Solar Cells Using Highly Conductive Polymer Anodes. *Adv. Mat.* (**2008**), 20, 4061-4067.
61. J. C. Gustafsson, O. Inganas, A. M. Andersson. Conductive polyheterocycles as electrode materials in solid state electrochromic devices. *Synth. Met.* (**1994**), 62, 17-21.
62. T. Smith, J. Guild. The C.I.E. colorimetric standards and their use. *Transactions of the Optical Society* (**1931**), 33, 73–134.

63. Y. Chen, J. Au, P. Kazlas, A. Ritenour, H. Gates & M. McCreary. Electronic paper: Flexible active-matrix electronic ink display. *Nature* (**2003**), 423, 138.

64. U. Resch-genger, et al. Quantum dots versus organic dyes as fluorescent labels. *Nature Method* (**2008**), 5, 763-775.

65. A. M. Chang, D. Aeschbach, J. F. Duffy, C. A. Czeisler. Evening use of light-emitting eReaders negatively affects sleep, circadian timing and next-morning alertness. *P. Natl. Acad. Sci. USA* (**2015)**, 112, 1232-1237.